Developing Flow and Heat Transfer in Strongly Curved Ducts of Rectangular Cross-Section

by

Gaymond Yee*

and

Joseph A. C. Humphrey**

Lawrence Berkeley Laboratory
University of California
Berkeley, California 94720

* Science Applications, Inc.
San Leandro, California

** Department of Mechanical Engineering
University of California
Berkeley, California 94720

Index

ABSTRACT

A numerical study of heat transfer in 90°, constant cross-section curved duct, steady, laminar flow is presented. The work is aimed primarily at characterizing the effects of duct geometry on heat transfer by considering, especially, the role of secondary motions during the developing period of the flow. However, due consideration has also been given to varying initial conditions of velocity and temperature at the entrance section to the duct. In addition, an assessment is made of the relative contributions of individual duct walls to heat transfer in the flow. It is found that, in general, heat transfer increases with Dean number with the largest transfer rates occurring through the duct side walls and outer-curvature wall. Duct geometries with aspect ratio greater or smaller than unity have weaker secondary motions and are less effective for heat transfer. Similarly, plug-flow entrance profiles for velocity retard the development of cross-stream flow thus inhibiting a significant contribution to heat transfer. It is concluded that short ducts with strong curvature ($2Rc/D_H < 10$) and intense secondary motions can be as effective for heat transfer as longer ducts which are less strongly curved.

Calculations are based on fully elliptic (in space) forms of the transport equations governing the flow. They are of engineering value and are limited in accuracy only by the degree of computational mesh refinement. A comparison with calculations based on parabolic equations has been made and it is shown how the latter can lead to erroneous results for strongly curved flows.

NOMENCLATURE

a	curved duct width
b	curved duct breadth
c_p	heat capacity at constant pressure
C_f	friction coefficient at ϕ plane
C_p	pressure loss coefficient at ϕ plane
De	Dean number $\left(Re\left(\frac{D_H/2}{Rc}\right)^{\frac{1}{2}}\right)$
D_H	curved duct hydraulic diameter (4x surface/perimeter)
h	perimeter average heat transfer coefficient at ϕ plane $(\bar{q}/(Tw-\bar{T}))$
k	thermal conductivity
Nu	perimeter average Nusselt number at ϕ plane $(\bar{h}D_H/k)$
P	pressure at a point in the flow
$\bar{P}$	surface average pressure at ϕ plane
Pr	Prandtl number $\mu c_p/k$
P_{ref}	P at $\theta = 0°$ plane
q_i	heat flux at a point on a wall
$\bar{q}$	perimeter average heat flux at ϕ plane
r	radial direction in cylindrical coordinates
r_i	inner curvature wall
r_o	outer curvature wall
Rc	duct radius of curvature $((r_i + r_o)/2)$
Re	Reynolds number $\left(\frac{D_H \cdot V_B}{\mu}\right)$
T	value of temperature at a point in the flow
$\bar{T}$	mass average temperature at ϕ plane
T_{in}	inlet temperature

T_w wall temperature

$|\vec{V}|$ modulus of secondary motion vector velocity at a point in the flow

V_B surface average longitudinal velocity at ϕ plane

v_ϕ longitudinal velocity component

v_r radial velocity component

v_z axial velocity component

z axial direction in cylindrical coordinates

θ non-dimensional temperature at a point in the flow $\left(\frac{T_w - T}{\bar{T}_w - T_{in}}\right)$

θ_B non-dimensional mass average temperature at ϕ plane $\left(\frac{\bar{T} - T_{in}}{\bar{T}_{in}}\right)$

μ viscosity

ρ density

τ_w wall shear stress

ϕ longitudinal direction in cylindrical coordinates

INTRODUCTION

Considerable effort has been expended on the experimental measurement and calculation of flows in curved ducts of rectangular cross-section, principally because of the practical significance of such flows. Curved duct geometries frequently arise in engineering configurations where, besides providing a necessary conduit for the fluid, it may be required to enhance heat and/or mass transport processes. In curved ducts this is achieved mainly due to the prolonged residence times of fluid elements which must move along spiraling paths as they evolve in the main (longitudinal) flow direction. Thus, the centrifugal force-radial pressure gradient imbalance acting on slow moving fluid near the side walls of the duct induces a motion of the fluid along the side walls and directed from the outer towards the inner curvature wall. In turn, faster moving fluid in the core region of the flow moves along the center (symmetry) plane of the duct, being directed from the inner to the outer curvature wall. The cross-stream motion just described is commonly referred to in the literature as secondary motion of the "first kind" or, simply, secondary motion [1]. It is obvious that the extent to which heat and mass transport can be enhanced in curved duct flows will be a strong function of the intensity and spatial variation of the secondary motion.

Even though experimental works on curved duct flows abound (a recent review may be found in [2]), data availability for engineering purposes is often defficient or simply inadequate. Whereas considerable work has been carried out to obtain useful design correlations for pressure losses and friction coefficients [3], there is no equivalent body of knowledge describing three-dimensional velocity, energy and mass transport phenomena

in sufficient detail and over a wide enough range of relevant dimensionless flow parameters. That this should be the case may be understood by considering the phenomenal task required only to obtain detailed measurements of three velocity components for different conditions of duct aspect ratio, Dean number, radius ratio $2Rc/D_H$ (for turbulent flows [4]) and, for developing flows, at various duct deflection angles. It is not surprising to find therefore that available velocity data is mainly restricted to the longitudinal component direction and that the majority of heat and mass transfer studies have focussed on cases of fully developed curved duct flow with boundary conditions of specific relevance to the particular cases investigated.

Whereas experimentation in curved duct geometries may be laborious (and complex), it is possible, in principle, to compute these flows quite accurately in the laminar regime. This has been shown by, among others, Cheng and Akiyama [5], Cheng, Lin and Ou [6] and Joseph, Smith and Adler [7] for fully developed flow and by Ghia and Sokhey [8] and Humphrey, Taylor and Whitelaw [9] for developing flow. Of the above only the procedure used by Humphrey, et. al. [9] is based on fully elliptic forms (in space) of the equations of motion. Calculations for turbulent flow regime have been performed by Pratap and Spalding [10] using a semi-elliptic numerical procedure. However, the agreement between calculations and measurements of velocity is less satisfactory in this case. Although the authors attribute the discrepancies to failings in the model of turbulence employed in the calculations, it is possible that their neglect of higher order curvature terms in the equations of motion may have contributed to the under-prediction of secondary velocity components.

Experimental investigations of heat transfer in curved duct flows have been described by, for example, Kreith [11], Mori, Uchida and Ukon [12]

and Yang and Liao [13] while corresponding numerical calculations are reported by Cheng and Akiyama [5] and Cheng, et. al. [6]. Except for the experimental works of Kreith [11] and Yang and Liao [13] (in turbulent regime) the remaining studies deal with the problem of fully developed laminar flow. In general, these and similar studies show that heat transfer in curved duct flow is enhanced relative to that occurring in straight ducts, with transfer rates at outer curvature walls being typically 2 to 5 times larger than corresponding values at inner walls. Non-dimensionalized values of temperature profiles show trends similar to those displayed by the longitudinal velocity component, with maximum values shifted towards the outer curvature wall. Equivalent information appears to be lacking for the case of developing laminar flow. Especially noticeable is the dearth of information for ducts with relatively strong curvature (small radius ratio: $2\ Rc/D_H \leq 10$) where spatial ellipticity in the flow field may be pronounced.

The present study is directed toward providing (through numerical computation) necessary fluid mechanical and heat transfer data for developing steady laminar flow of an incompressible fluid in strongly curved ducts with 90° deflection angle. The calculations are of engineering accuracy and allow a relative comparison of duct performance and detailed flow characteristics as a function of relevant dimensionless parameters, such as Dean and Reynolds number, aspect ratio and radius ratio. Because of the numerical approach in the study it has been possible to examine an extensive combination of geometrical configurations for various initial and boundary conditions for temperature and velocity. The experimental equivalent of this (or a similar) study would be exceedingly laborious, time consuming and expensive to perform. This substantiates

the need for developing and applying calculation procedures which can be used with confidence, relatively easily and (by comparison to experiments) at moderate costs. The numerical procedure used in this study is presently the basis for similar calculations in turbulent single and two-phase flow to be reported at a later date.

CALCULATION PROCEDURE AND TEST CASES

The calculation procedure used to compute the flows in this study has already been described in [9]. Extension of the procedure to arbitrary orthogonal coordinate geometries and, especially, its application to developing curved pipe flows of strong curvature have been documented by Humphrey [10]. The latter reference contains general finite difference forms of the conservation equations for mass, momentum and transferable scalar quantities (species and energy). Detailed information concerning the derivation of the difference equations, their numerical solution and results for various test cases solved to evaluate the procedure are reported in the above two references and in [2]. This section presents a summary of the essential features characterizing the calculation method together with a description of its application to flows in curved ducts with heat transfer. Some of the results for two calculated test cases are also reported.

Equations, Boundary Conditions and Procedure for Numerical Solution

Mass conservation, momentum and energy equations for three-dimensional, steady, incompressible laminar flow in curved ducts of cylindrical geometry corresponding to Fig. 1 are given by

$$\frac{\partial v_r}{\partial r} + \frac{1}{r}\frac{\partial v_\phi}{\partial \phi} + \frac{\partial v_z}{\partial z} + \frac{v_r}{r} = 0 \quad . \tag{1}$$

$$\left[v_r \frac{\partial v_r}{\partial r} + \frac{v_\phi}{r}\frac{\partial v_r}{\partial \phi} + v_z \frac{\partial v_r}{\partial z} - \frac{v_\phi^2}{r} \right] = -\frac{\partial p}{\partial r} + \mu \left[\nabla^2 v_r - \frac{v_r}{r^2} - \frac{2}{r^2}\frac{\partial v_\phi}{\partial \phi} \right] . \tag{2}$$

$$\left[v_r \frac{\partial v_\phi}{\partial r} + \frac{v_\phi}{r}\frac{\partial v_\phi}{\partial \phi} + v_z \frac{\partial v_\phi}{\partial z} + \frac{v_r v_\phi}{r} \right] = -\frac{1}{r}\frac{\partial p}{\partial \phi} + \mu \left[\nabla^2 v_\phi + \frac{2}{r^2}\frac{\partial v_r}{\partial \phi} - \frac{v_\phi}{r^2} \right] \tag{3}$$

$$\rho\left[v_r\frac{\partial v_z}{\partial r} + \frac{v_\phi}{r}\frac{\partial v_z}{\partial \phi} + v_z\frac{\partial v_z}{\partial z}\right] = -\frac{\partial p}{\partial z} + \mu\nabla^2 v_z \tag{4}$$

$$\rho\, c_p\left[v_r\frac{\partial T}{\partial r} + \frac{v_\phi}{r}\frac{\partial T}{\partial \phi} + v_z\frac{\partial T}{\partial z}\right] = k[\nabla^2 T] \tag{5}$$

where

$$\nabla^2 = \frac{\partial^2}{\partial r^2} + \frac{1}{r}\frac{\partial}{\partial r} + \frac{1}{r^2}\frac{\partial^2}{\partial \phi^2} + \frac{\partial^2}{\partial z^2} \tag{6}$$

It is required to solve (1)-(5) together with various combinations of the boundary conditions as shown below:

Inlet plane ($\phi = 0°$).

$v_r = v_z = 0$, v_ϕ = plug flow or developed duct flow (7)

T = constant or $f(r)$

Exit plane (all r and z at $\phi = 90°$).

$$\frac{\partial v_r}{\partial \phi} = \frac{\partial v_z}{\partial \phi} = \frac{\partial v_\phi}{\partial \phi} = \frac{\partial T}{\partial \phi} = 0 \tag{8}$$

with overall continuity of mass and energy imposed.

Side walls (all ϕ at $z = \pm b/2$ and $r = r_i, r_o$).

$v_r = v_z = v_\phi = 0$ (9)

T = constant or $f(\phi)$ at specified walls

$q = 0$ at specified walls

Symmetry plane (all r and ϕ at $z = 0$).

$$v_z = \frac{\partial v_r}{\partial z} = \frac{\partial v_\phi}{\partial z} = \frac{\partial T}{\partial z} = 0 \tag{10}$$

The conditions imposed for velocity at the inlet and exit planes have been carefully discussed in [14]. It is shown there that the curved duct has a minimal effect on the incoming fluid stream, thus allowing a fairly arbitrary prescription of the velocity distribution at $\zeta = 0°$. While not strictly correct, the velocity condition at the exit plane ($\zeta = 90°$) is a good approximation and is substantiated by the satisfactory agreement found here (and in [9,14]) between measurements and calculations.

The finite difference equations are obtained by integrating (1)-(5) over volume elements or "cells" discretizing the flow domain. The velocity components, pressure and temperature are the dependent variables computed on a number of staggered, interconnected grids, each of which is associated with a specific variable. The general form of the finite difference expression is given by

$$\phi_P = \left(\sum_{i=1}^{6} A_i \phi_i + S_o \right) \Big/ \sum_{i=1}^{6} A_i \qquad (11)$$

where ϕ_P (velocity component, pressure or temperature) is the variable solved for at a position P in the discretized flow domain. The A_i coefficients are determined at the cell surfaces and represent the combined contributions of convection and diffusion to the balance of ϕ. Other contributions arising from pressure, body forces and temperature (sources or sinks) are contained in S_o. Detailed forms for S_o in variable property flows are available in [15].

Solution of the system of finite difference transport equations with appropriately differenced boundary conditions is achieved by means of a cyclic series of predictor-corrector operations as described in [9,14]. Briefly, the method involves using an initial or intermediate value of the

pressure field to solve for an intermediate velocity field. A pressure correction to the pressure field is determined by bringing intermediate velocities into conformity with continuity. Corrections to the pressure and velocity fields are applied and the energy equation is solved for T (in flows where energy and momentum are not linked through temperature effects this last step can be taken after the velocity and pressure fields have been determined). The above steps are repeated until some pre-established convergence criterion is satisfied.

Test Cases

Extensive testing and an evaluation of the calculation procedure for predicting flows without heat transfer have been documented in [2] and reported in part in [9,14]. It has been shown in these references that fully elliptic, three-dimensional computations of sufficient accuracy for engineering purposes can be obtained on unequally spaced grids as coarse as 12 x 12 x 20 ($r \times z \times \phi$). The predictions presented here and in the following sections have been performed on a 12 x 15 x 20 mesh. While finer grids are capable of yielding more accurate results, they are increasingly more expensive to compute. Whereas numerical schemes based on parabolic or semi-elliptic forms of the transport equations will handle equivalent and finer calculation meshes at significantly less cost, for flows such as the ones of interest here where curvature effects can be pronounced, it is not possible to determine a priori if less than fully elliptic equations are justified. For two interesting examples involving flow reversal in curved ducts, see [9,14].

Profiles of longitudinal velocity and pressure, respectively calculated with elliptic and parabolic forms of the transport equations, are shown (Fig. 2(a-c) where they are compared with experimental velocity data from

[9]. The parabolic calculations were readily obtained by modifying the elliptic procedure of [9,14] as explained in, for example, Launder [16]. The plots allow a relative comparison between the two approaches for a duct of relatively strong curvature (case 1 in Table 1). It can be seen that the elliptic results yield significantly better predictions of longitudinal velocity (and cross-stream components not shown here), especially between $\phi = 30°$ and $\phi = 90°$ where elliptic effects are strongest. The pressure profiles in Fig. 2-c show, in part, the reason for the discrepancy. In the parabolic calculations pressure links in the longitudinal direction are decoupled and lead to over-predicted values at $r = r_0$ and under-predicted values at $r = r_i$. Thus, even though the velocity field is "parabolic" in that it contains no reversed flow zones, ellipticity in the pressure field is still strong and must be dealt with accordingly.

Additional indications of the differences which can arise between elliptic and parabolic computational approaches in strongly curved flows may be gleaned from a comparison of the results presented for velocity components and temperature in Figs. 4-a and 4-b, respectively. The figures contain plots of calculated results at $\phi = 90°$ which are significantly dissimilar. In particular, the parabolic longitudinal velocity contours show high speed fluid trapped near the outer curvature wall between the side wall and symmetry plane. This effect contradicts experimental evidence in [9] and is due to the over-prediction of an unfavorable longitudinal pressure gradient at the outer curvature wall. The over-prediction also explains why secondary motion at the outer radius wall, near the symmetry plane, is directed away from the wall and into the flow. Of course, differences in the temperature contours will arise because of the differences in velocity and will be in error as well. It may be concluded that for

developing curved duct flows with De < 250, significant error can arise through the use of parabolic schemes. All the calculations performed for the parametric study presented in the next section have been based on fully elliptic forms of the transport equations as given in (1)-(5).

As a check for the validity of the calculation procedure in the presence of heat transfer effects, numerical computations were performed for two of the experimental cases presented by Mori, et. al. [12] for fully developed curved duct flow. The agreement between calculations and measurements can be judged from the profiles for velocity and temperature shown in Fig. 3. It is considered to be satisfactory given the uncertainty reported in connection with the experiments which were affected by the presence of large turbulence fluctuations at the entrance section of the curved duct. It is shown in [2] that the largest turbulent fluctuations in curved square duct flow arise at the outer curvature wall. The fluctuations will contribute to turbulent diffusion from the wall region into the core flow and can account for the lower experimental values of temperature found in [12] at the outer radius wall.

Rigorously, the procedure should be tested for its capacity to predict momentum and heat transfer effects during the developing period of duct flow. However, the authors are unaware of any experimental data in curved ducts which would serve for such a comparison. Notwithstanding, calculations performed for developing temperature profiles in straight duct flow show excellent agreement with experimental measurements and analytical results. For this and more detailed discussion of the test cases reported here see Yee [17].

CASE STUDIES, RESULTS AND DISCUSSION

A summary of the case studies and conditions calculated for this investigation is presented in tabulated form in Table 1. From the table it will be seen that various curved duct geometries were combined with parabolic (fully developed straight duct flow) profiles for velocity and uniform temperature (T_{in} = 300°K) distributions at the entrance plane (ζ = 0°). The effects of varying initial temperature and velocity distribution were also investigated. Finally, the effects of heating curved duct walls singly, with adiabatic conditions imposed for the remaining walls, were explored. In all cases the boundary condition was that of constant wall temperature (T_w = 350°K) except for where the adiabatic condition was enforced. Although not calculated here, variable wall temperature or variable (or constant) heat flux conditions could have just as readily been specified at the boundaries.

Incompressible, constant property (Pr = 1.0) flow was assumed for the calculations and is an acceptable supposition for the range of temperatures considered here. While the calculation of temperature dependent fluid properties is a standard feature in the numerical procedure, it does increase the cost of predictions through additional storage and computing time requirements. Typical values for storage and CP times for the case studies presented here were 160 K_8 and 235 seconds, respectively on a CDC 7600. The average time required per node x iteration for all runs was 1.44 x 10^{-5} CP seconds.

The remainder of this section is devoted to the presentation and and discussion of some of the results calculated for the test cases in Table 1. The presentation is subdivided according to the topic of interest both for ease of discussion and to enhance the separate roles of the various parameters affecting heat transfer in curved duct flow.

1 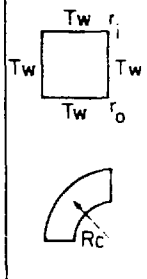 b/a = 1 Rc/DH = 2.3 Re = 790 De = 368 Tin = 300° K Tw = 350° K	**1A** 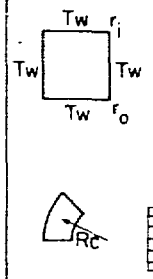 b/a = 1 Rc/DH = 4.6 Re = 790 De = 260 Tin = 300° K Tw = 350° K	**2** 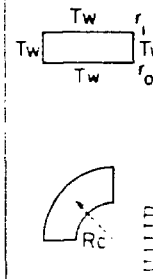 b/a = 3 Rc/DH = 2.3 Re = 790 De = 368 Tin = 300° K Tw = 350° K	**3** 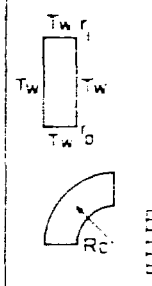 b/a = 1/3 Rc/DH = 2.3 Re = 790 De = 368 Tin = 300° K Tw = 350° K	**4** 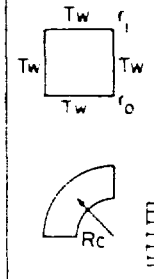 b/a = 1 Rc/DH = 1 Re = 150 De = 106 Tin = 300° K Tw = 350° K
5 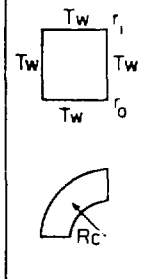 b/a = 1 Rc/DH = 2.3 Re = 150 De = 70 Tin = 300° K Tw = 350° K	**6** 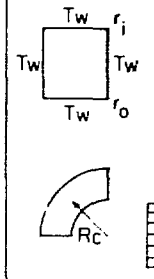 b/a = 1 Rc/DH = 4 Re = 150 De = 53 Tin = 300° K Tw = 350° K	**7** 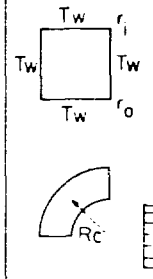 b/a = 1 Rc/DH = 2.3 Re = 790 De = 368 Tin = 300° K Tw = 350° K	**8** 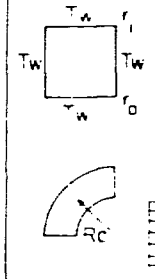 b/a = 1 Rc/DH = 2.3 Re = 790 De = 368 Tin = 300° K Tw = 350° K	**9** 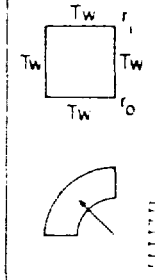 b/a = 1 Rc/DH = 2.3 Re = 790 De = 368 Tin = 300° K Tw = 350° K
10 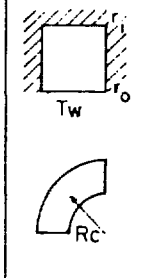 b/a = 1 Rc/DH = 2.3 Re = 790 De = 368 Tin = 300°K Tw = 350°K	**11** 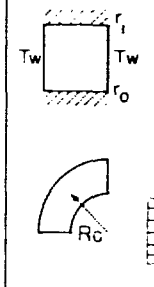 b/a = 1 Rc/DH = 2.3 Re = 790 De = 368 Tin = 300°K Tw = 350°K	**12** 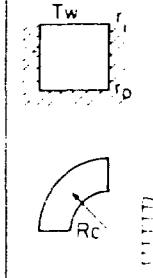 b/a = 1 Rc/DH = 2.3 Re = 790 De = 368 Tin = 300°K Tw = 350°K	**13** PARABOLIC TEST CASE Equivalent to Case 1, but using a parabolic procedure	

Table 1. Calculated case studies.

Velocity and Temperature Distributions

Plots of non-dimensional velocity and temperature distributions are given in Fig. 4(a-h). Longitudinal velocity and temperature are shown in the form of equal-value contours whereas the cross-stream motion is indicated in vectorial form.

Bend angle (ϕ).

The distributions shown in the figures are typical of the bulk of the results and illustrate clearly the important role played by secondary motions insofar as heat and momentum transport are concerned. Thus, for example, the sequence shown in Fig. 4-a,b,c provides a clear impression of the way the flow and temperature fields evolve to produce maximum values in the respective distributions displaced toward the outer-radius wall. The similarity between longitudinal velocity and temperature contours is striking but not surprising in view of the convective nature of the flow. The energy field is decoupled from the momentum field and in all cases evolves in a manner dictated primarily by the fluid mechanics.

Aspect ratio (b/a).

The effect of varying aspect ratio may be shown by a relative comparison of Fig. 4-c,d,e. It is immediately obvious that the vector plots for cross-stream velocity differ considerably depending on the aspect ratio. For b/a = 1 the secondary motion is relatively high in the region of the inner-curvature ($r = r_i$) and side ($z = b/2$) walls, whereas for b/a = 3 it is high at all three walls but localized mainly in the region of the side wall. For b/a = 1/3 the cross-stream flow is intense along both the duct symmetry plane and side walls but, by comparison, is relatively weak at the inner- and outer-curvature walls. Longitudinal velocity and temperature

contours show distributions corresponding to the sense of the secondary motion. For b/a = 1/3 it is worth remarking on the peak value of longitudinal velocity which has been displaced from the duct symmetry plane whence it evolved. A corresponding peak in the temperature distribution is not observed. In addition, for this last case, longitudinal velocity and temperature profiles are most dissimilar and is probably due to a relatively large contribution to heat transfer through conduction along the z axis.

Velocity entrance condition.

The effect of a plug flow entrance condition may be assessed by comparing Figs. 4-c and f. Secondary flow evolves considerably more slowly in the case of a flat profile entrance condition and is to be expected since the boundary layers on the side walls, where the transverse pressure gradient has its strongest effect, are initially very thin. As a consequence both the longitudinal velocity and temperature develop slowly also. Although not shown here, the longitudinal velocity for this case was observed to develop a potential-flow-like appearance over the first 20 to 30 degrees in the duct. While this effect is hardly noticeable at $\zeta = 90°$, remnants of its presence may be detected in the temperature profiles which display double maxima near the inner-radius wall.

Individually heated walls.

Figure 4-g shows temperature distributions at 90° for three cases in Table 1 where only one of the two curved walls or both of the side walls were heated while keeping the remaining walls adiabatic. The fluid mechanics of these cases are identical to Figs. 4-a, b and c but the manner in which the temperature fields evolve are strikingly different. In all cases the

calculations show graphically how the secondary motion scoops warm fluid from the vicinity of the heated wall and convects it in the sense of the secondary motion. It would appear that this is achieved most successfully for case II with heat flowing into the duct through the side walls. The point that emerges clearly from the comparison is that heat transfer rates through the three types of walls present in curved duct flow can, and in general will, differ markedly depending on flow conditions, geometrical characteristics and fluid properties.

Pressure loss (C_p) and friction (C_f) coefficients.

Profiles for the pressure loss and friction coefficients corresponding to the case studies in Table 1 are given in Figs. 5(a) and (b). C_p is seen to decrease with increasing duct angle ϕ and decreasing De, and (from the trend in the results at ϕ = 1.5 radians) with decreasing b/a. The C_p curve for the plug flow entrance profile is also plotted for comparison with the other cases.

In all cases the friction coefficient at the outer wall ($r = r_o$) increases (at least initially) with increasing duct angle. However, the rate of increase is largest for b/a = 1 and smallest for b/a = 1/3. High values of C_f at $r = r_o$ are initially favored by low values of De but the reverse is true for $\phi \gtrsim 1.2$ radians. At the inner curvature wall C_f appears to be relatively insensitive to changes in De and for $\phi \gtrsim .7$ is largest for b/a = 3. The potential flow profiles show C_f decreasing at $r = r_o$ and increasing at $r = r_i$, respectively and is due to the boundary layer growth occurring on these walls.

Variation of temperature and Nusselt number.

Figures 6-a, b and c show the effects of duct geometry, flow characteristics and duct entrance conditions on normalized temperature and

Nusselt number, respectively. In the plots the Nusselt number has been calculated from

$$N_u = \frac{\bar{h} D_H}{\bar{k}} \tag{7}$$

where h is the (local) heat transfer coefficient averaged over the duct perimeter at a duct angle ζ. Thus,

$$h = q/(T_w - \bar{T}) \tag{8}$$

where q is the (perimeter) averaged heat flux at the ζ plane and T_w and $\bar{T}$ are the wall temperature and average flow temperatures, respectively, at the same longitudinal position.

The curves in Fig. 6-a all show $\bar{N}u$ increasing asymptotically with duct arc-length, after an initial and rather abrupt period of decay. The initial decrease in $\bar{N}u$ is due to the relatively weak mixing effect of the secondary motion during this stage of the flow. However, as the flow develops and the intensity of the secondary motion increases, heat transfer is enhanced and $\bar{N}u$ increases with ζ. The minima in the curves are seen to depend on the value of De and, in general, $\bar{N}u$ increases with increasing De. Initially, the average temperature of fluid in the ducts appears to be insensitive to variation in the De number. Eventually, however,

secondary motions in the shorter but more strongly curved duct (De = 106) enhance heat transfer to the point where a definite trend in the temperature profiles emerges. It may be concluded therefore that, for certain conditions, short ducts with intense secondary motion can transfer as much heat or more compared to ducts of longer length but with weaker cross-stream flow. That this is indeed the case was independently confirmed by performing total heat balances for cases 1 and 1A in Table 1. Thus, for conditions of equal arc length, 1.15 times more heat was added to the duct with higher De.

From Fig. 6-b it is seen that Nu is highest for b/a = 1 for $\zeta > .4$ radians. It would appear that initial heat transfer gains through increased surface area are eventually offset by reductions due to weaker cross-stream flows for both b/a = 3 and b/a = 1/3. The plots also show that temperature gradients at the outer radius wall have a more pronounced effect on the rate of heat transfer than corresponding gradients at the inner wall. This is partly due to a surface effect but also to the presence of higher gradients of velocity at the outer radius wall.

In order to assess the relative contributions to heat transfer arising from separate duct walls during flow development, calculations were performed for the conditions corresponding to cases 10-12 in Table 1. The results for $\bar{Nu}$ and $\bar{Nu}_B$ are shown in Fig. 6-c. If allowance is made for the difference in wall areas among the cases the plots still indicate that the highest rates of heat transfer occur through the side and outer radius walls in curved duct flow. This result is linked to the high values of secondary motion which arise, especially in the vicinity of the side walls, and is the cause for the pronounced maximum in the Nu plot corresponding to case 11. By

comparison similar variations and maximum values of $\bar{Nu}$ are less for the case of heat transfer through the inner curvature wall. Energy balances for these three cases show that the total heat added to the duct heated through the outer wall was 1.58 times larger than that added to the duct heated through the inner wall. In turn, the total heat added to the duct heated through the side walls (allowing for the fact that there were two) was 1.02 times larger than that added to the duct heated through the outer wall.

CONCLUSIONS

The following major conclusions are derived from the present study:

1. Secondary motions in developing curved duct flow are largely responsible for enhanced rates of heat transfer after an initial period transpires to allow significant development of the cross-stream flow. In the present study this period corresponded to a bend angle of $30° < \phi < 50°$ approximately.

2. Short ducts with strong curvature may transfer as much or more heat (to a moving fluid in which the secondary motion is intense) as longer ducts which are not as strongly curved (and in which the secondary motion is weaker).

3. Higher rates of heat transfer are favored by large De, $b/a = 1$, parabolic velocity entrance conditions, and large temperature and velocity gradient conditions at outer curvature and side walls, respectively.

4. For a plug-flow entrance velocity condition initial heat transfer rates are large but are subsequently reduced (quite considerably) due to the much slower development of the cross-stream flow.

5. Whereas high values of De number favor large heat transfer rates, the advantage must be weighed against corresponding increases in friction losses.

6. Flows in curved ducts with strong curvature require a fully elliptic numerical treatment to yield satisfactory computations. Calculations based on parabolic forms of the transport equations can produce erroneous results.

In general, the study shows that heat transfer in developing curved duct laminar flow can be usefully and comprehensively investigated through numerical computation of finite difference transport equations. The results obtained are of sufficient accuracy for engineering use and are limited in resolution only by the degree of mesh refinement imposed in the calculations. Equivalent experiments would be laborious, time consuming and expensive to perform.

The calculation procedure used for this work is presently the basis for turbulent single and two-phase flow predictions in curved duct geometries. Because of the high turbulence fluctuations observed at the curved and side walls in these flows [2], it is anticipated that contributions through turbulent diffusion of particles and/or heat will significantly influence scalar transport even though the fluid mechanics appear to be dictated primarily by pressure gradient and body force field effects.

ACKNOWLEDGEMENTS

Financial support for the numerical calculations performed during the course of this work was provided by the Division of Materials Sciences, Office of Basic Energy Sciences, U.S. Department of Energy under contract number W-7405-ENG-48. The authors welcome the opportunity to express their appreciation for this support. We are also grateful to Mr. R. Wylie for providing the results corresponding to the parabolic flow test case.

REFERENCES

1. BRADSHAW, P., ed., Turbulence, 2nd ed., Vol. 12, Topics in Applied Physics, Springer-Verlag, New York, 1978, pp. 118-123.

2. HUMPHREY, J.A.C., "Flow in Ducts with Curvature and Roughness," Ph.D. Thesis, University of London, 1977.

3. WARD-SMITH, A.J., "Pressure Losses in Ducted Flows," Butterworth, London, 1971.

4. ITO, H., "Friction Factors for Turbulent Flow in Curved Pipes," Trans. ASME, J. Bas. Eng., Vol. 11, 1959, pp. 123.

5. CHENG, K.C., and AKIYAMA, M., "Laminar Forced Convection Heat Transfer in Curved Rectangular Channels," Int. J. Heat Mass Transfer, Vol. 13, 1970, p. 471.

6. CHENG, K.C., LIN, R.C. and OU, J.W., "Graetz Problem in Curved Rectangular Channels with Convective Boundary Conditions - The Effect of Secondary Flow on Liquid Solidification - Free Zone," Int. J. Heat Mass Transfer, Vol. 18, 1975, p. 996.

7. JOSEPH, B., SMITH, E.P., and ADLER, R.J., "Numerical Treatment of Laminar Flow in Helically Coiled Tubes of Square Cross-Section," A.I.Ch.E.J., Vol. 21, No. 5, 1975, p. 965.

8. GHIA, K.N. and SOKHEY, J.S., "Laminar Incompressible Viscous Flow in Curved Ducts of Rectangular Cross-Sections," Trans. ASME, J. Fluids, Eng. 1, Vol. 99 , 1977, pp. 640-648.

9. HUMPHREY, J.A.C., TAYLOR, A.M.K., and WHITELAW, J.H., "Laminar Flow in a Square Duct of Strong Curvature," J. Fluid Mech., Vol. 83, Part 3, 1977, pp. 509-527.

10. PRATAP, V.S. and SPALDING, D.B., "Numerical Computation of the Flow in Curved Ducts," Aeronaut. Quart., Vol. 26, 1975, p. 219.

11. KREITH, F., "The Influence of Curvature on Heat Transfer to Incompressible Fluids," Trans. ASME, Vol. 77, 1955, p. 1247.

12. MORI, Y., UCHIDA, Y., and UKON, T., "Forced Convective Heat Transfer in a Curved Channel with a Square Cross-Section," Int. J. Heat Mass Transfer, Vol. 14, 1971, p. 1787.

13. YANG, J.W. and LIAO, N., "Turbulent Heat Transfer in Rectangular Ducts with 180° Bend," Proceedings of the 5th International Heat Transfer Conference, J.S.M.E., 1974, p. 169.

14. HUMPHREY, J.A.C., "Numerical Calculations of Developing Laminar Flow in Pipes of Arbitrary Curvature Radius," Can. J. Chem. Eng., Vol. 56, 1978, pp. 151-164.

15. HUMPHREY, J.A.C., "Numerical Calculation of Variable Property Flows in Curvilinear Orthogonal Coordinates," Can. J. Chem. Eng., Vol. 56, 1978, pp. 624-626.

16. LAUNDER, B.E., ed., Studies in Convection, Vol. 1, Academic Press, New York, 1975, pp. 1-78.

17. YEE, G., "Heat Transfer in Strongly Curved Duct Flow," Mech. Eng. Project Report, University of California, Berkeley, 1979.

FIGURE CAPTIONS

Fig. 1 Curved duct cylindrical coordinate geometry.

Fig. 2-a,b Comparison of elliptic (-) and parabolic (---) calculations with experimental (O) measurements of longitudinal velocity. Measurements are from Humphrey, et. al. [9]. (a): z/(b/2) = 0; (b): z/(b/2) = 0.5.

Fig. 2-c Comparison of elliptic (--) and parabolic (---) calculations of pressure at inner and outer curvature walls.

Fig. 3-a,b Calculated (-) and measured (o,Δ) longitudinal velocity. Experiments are from Mori, et. al. [12]. (a): $K = \sqrt{2}\,De = 389$; (b) $K = \sqrt{2}\,De = 876$.

Fig. 3-c,d Calculated (-) and measured (o,Δ) temperature. Experiments are from Mori, et. al. [12]. τ is wall temperature gradient. 0.49°C/cm. (c): $K = \sqrt{2}\,De = 389$; (d): $K = \sqrt{2}\,De = 876$.

Fig. 4-a Longitudinal velocity (V_ϕ/V_B), secondary motion ($\vec{V}/V_B$) and temperature θ at $\phi = 0°$ for Case 1 in Table 1.

Fig. 4-b Longitudinal velocity (V_ϕ/V_B), secondary motion ($\vec{V}/V_B$) and temperature θ at $\phi = 45°$ for Case 1 in Table 1.

Fig. 4-c Longitudinal velocity (V_ϕ/V_B), secondary motion ($\vec{V}/V_B$) and temperature θ at $\phi = 90°$ for Case 1 in Table 1.

Fig. 4-d Longitudinal velocity (V_ϕ/V_B), secondary motion ($\vec{V}/V_B$) and temperature θ at $\phi = 90°$ for Case 2 in Table 1.

Fig. 4-e Longitudinal velocity (V_ϕ/V_B), secondary motion ($\vec{V}/V_B$) and temperature θ at $\phi = 90°$ for Case 3 in Table 1.

Fig. 4-f Longitudinal velocity (V_ϕ/V_B), secondary motion ($\vec{V}/V_B$) and temperature θ $\phi = 90°$ for Case 7 in Table 1.

Fig. 4-g Temperature at 90° for Cases 10, 11 and 12 in Table 1.

Fig. 4-h Longitudinal velocity (V_ϕ/V_B), secondary motion ($\vec{V}/V_B$) and temperature θ at $\phi = 90°$ for Case 13 in Table 1 .

Fig. 5-a Pressure loss curves for case studies in Table 1.

Fig. 5-b Friction coefficient curves for case studies in Table 1.

Fig. 6-a Longitudinal variation of Nusselt and temperature for different De.

Fig. 6-b Longitudinal variation of Nusselt for different b/a (Cases 1,2,3) and for different temperature and velocity entrance conditions (Cases 7,8,9).

Fig. 6-c Longitudinal variation of Nusselt and temperature for individually heated walls.

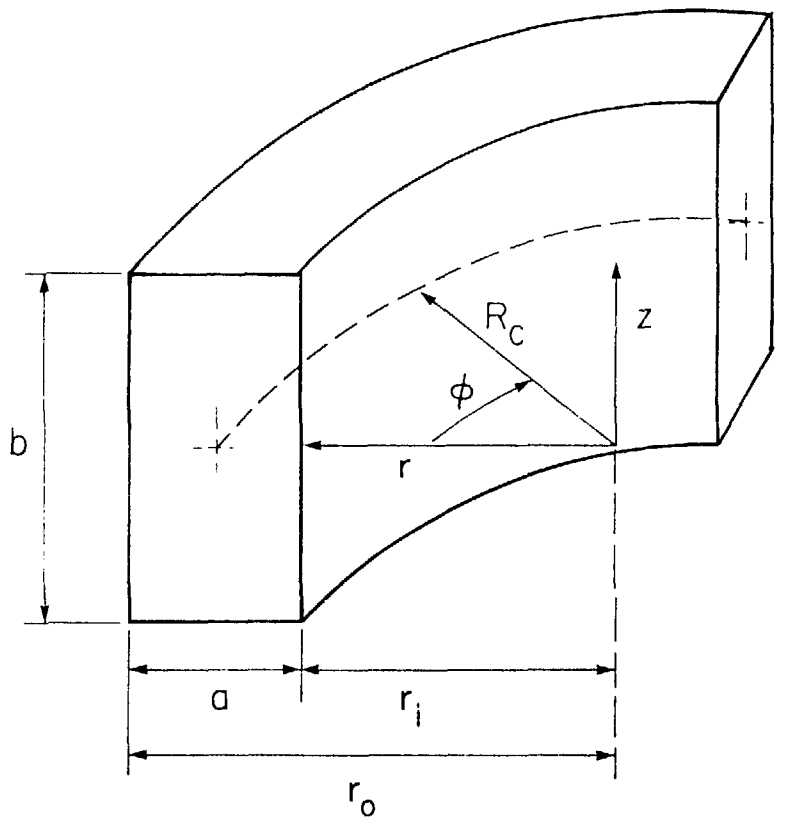

FIGURE 1

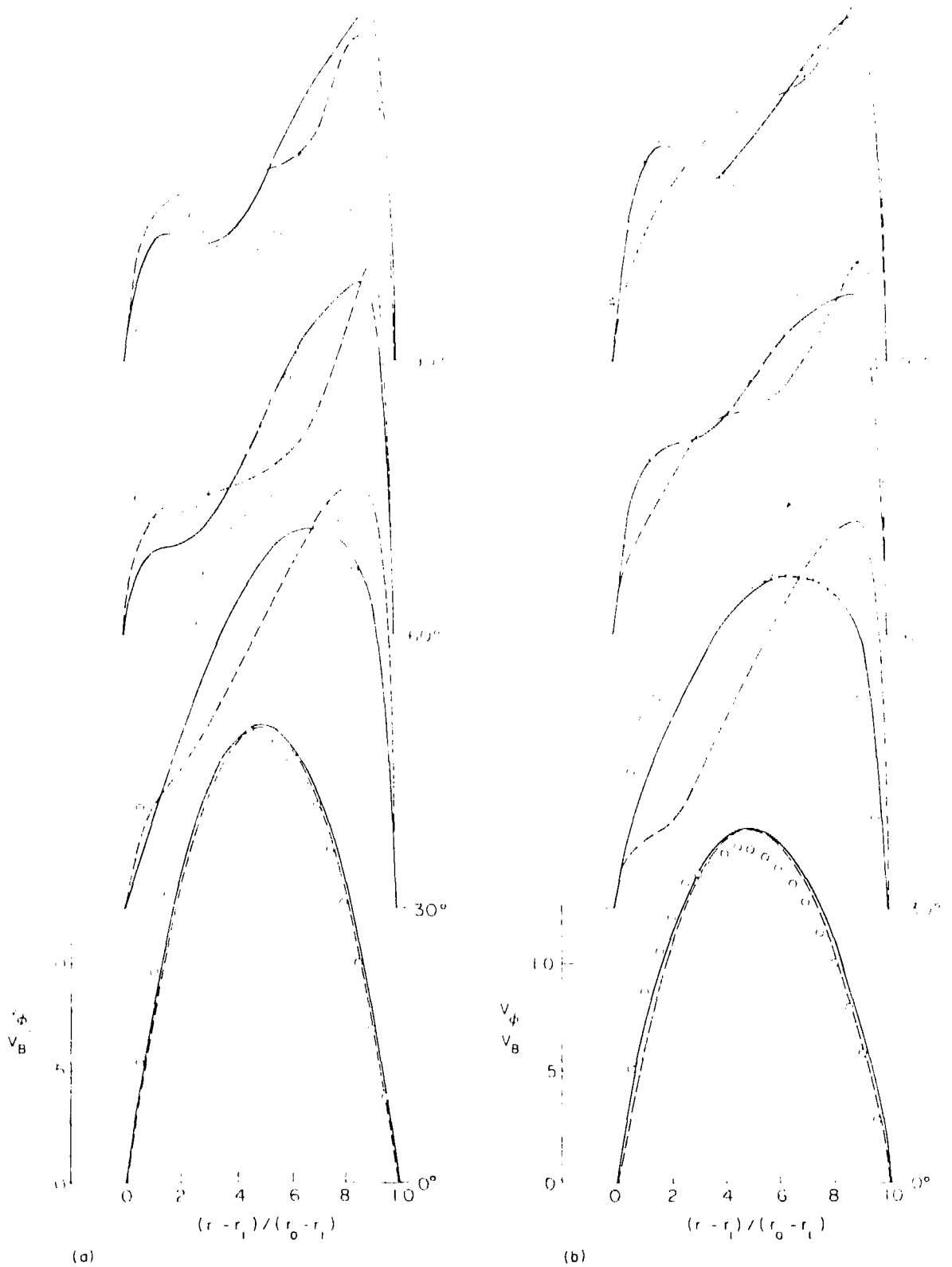

FIGURE 2-a,b

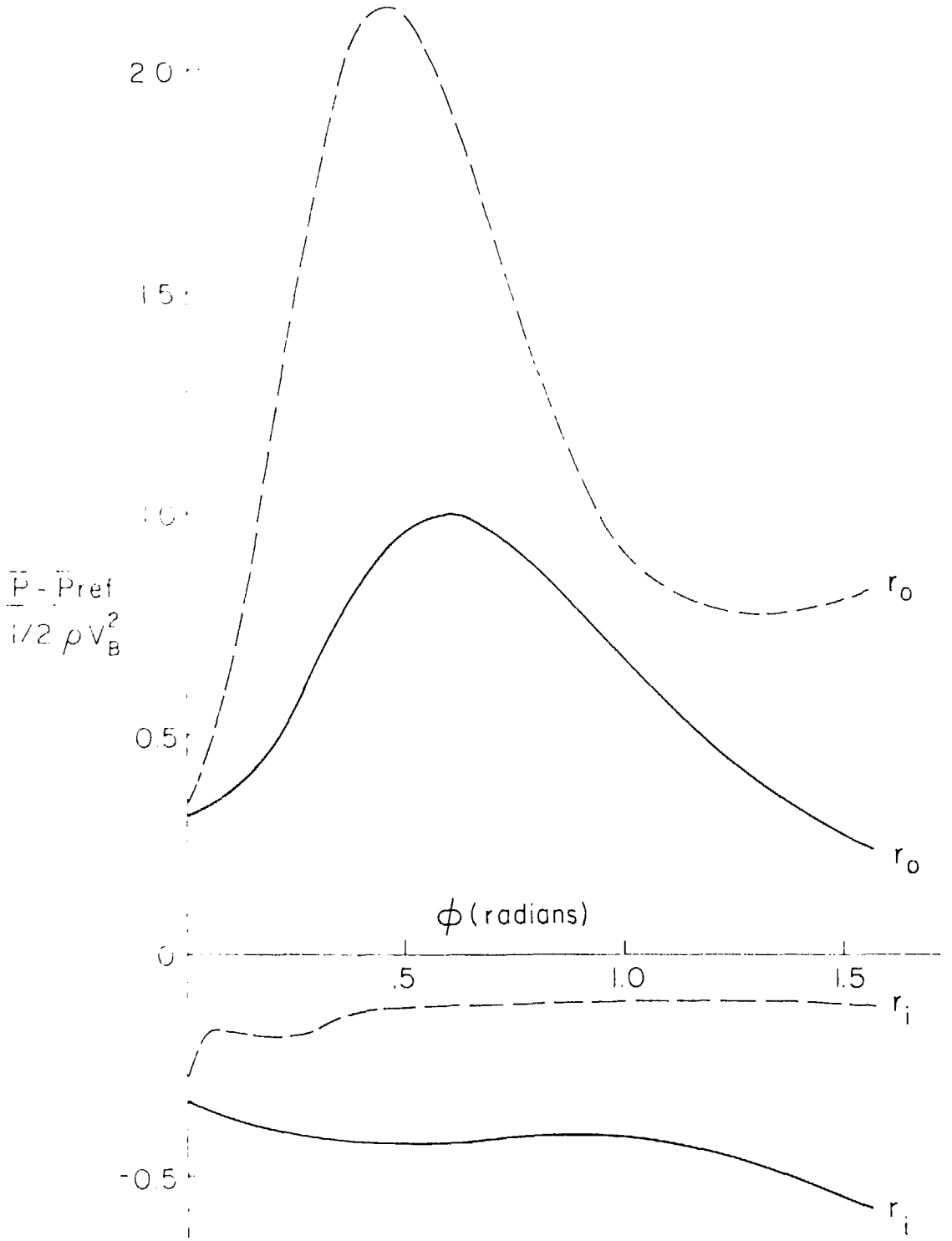
2.0
1.5
1.0
0.5
0
-0.5
$\frac{\bar{P} - \bar{P}_{ref}}{1/2\,\rho V_B^2}$
ϕ (radians)
.5
1.0
1.5
r_o
r_o
r_i
r_i

FIGURE 2-c

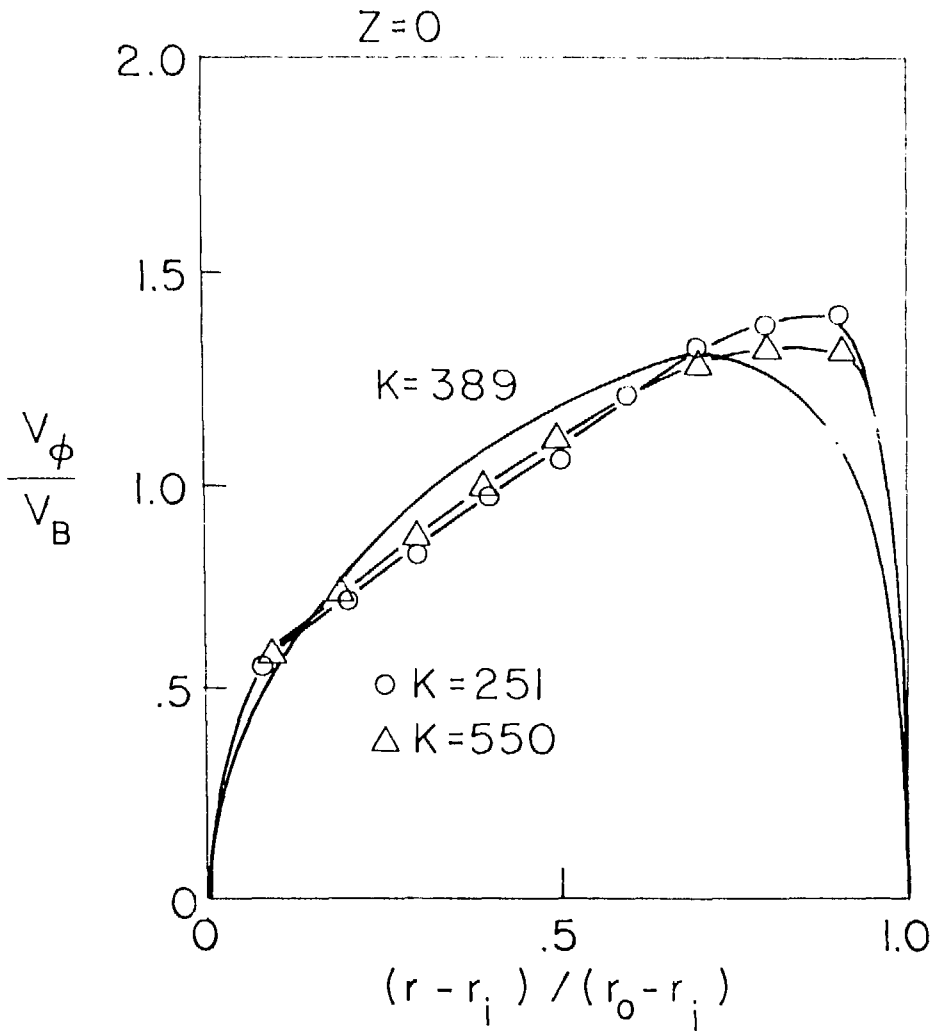

FIGURE 3-a

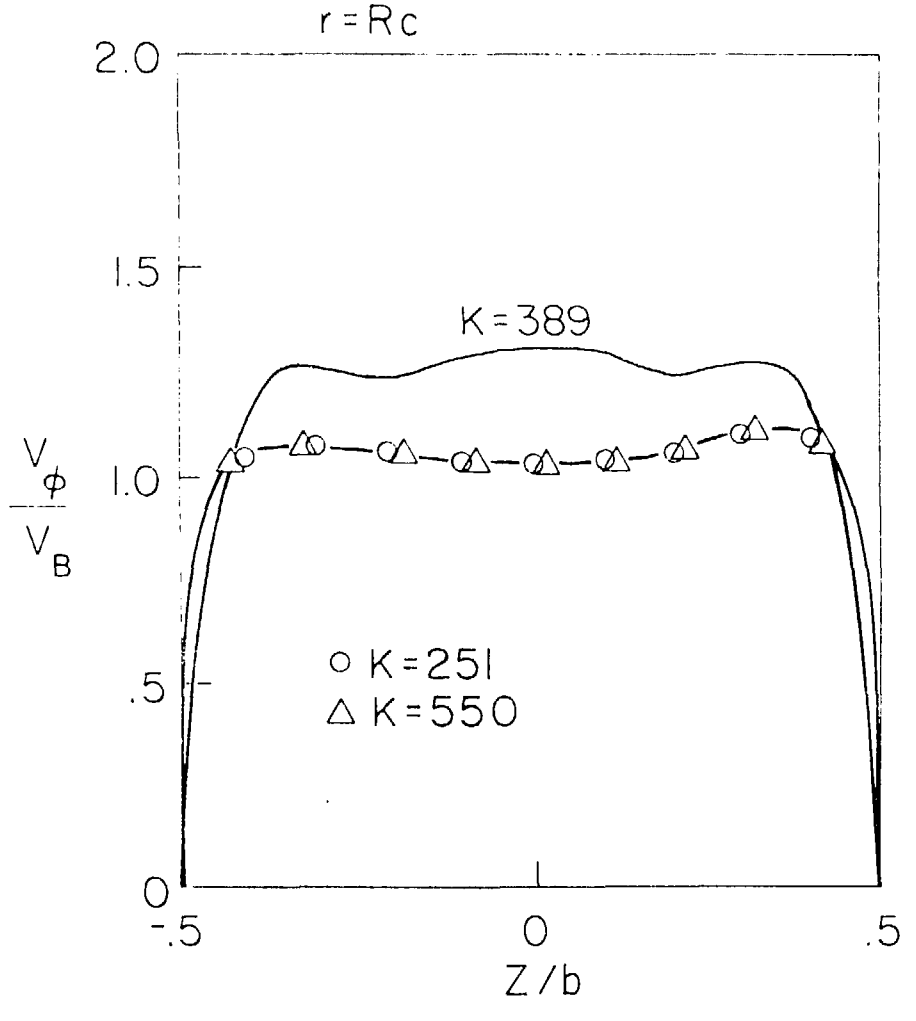

FIGURE 3-a

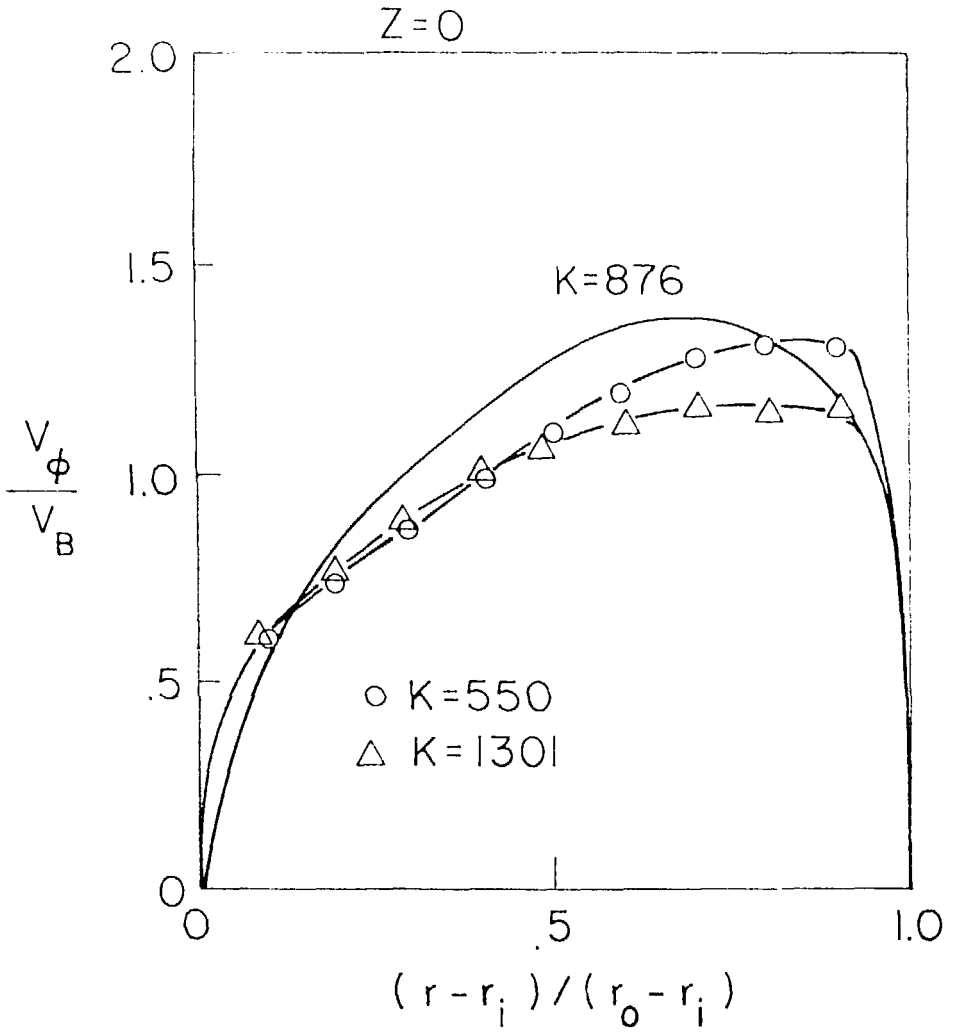

FIGURE 3-b

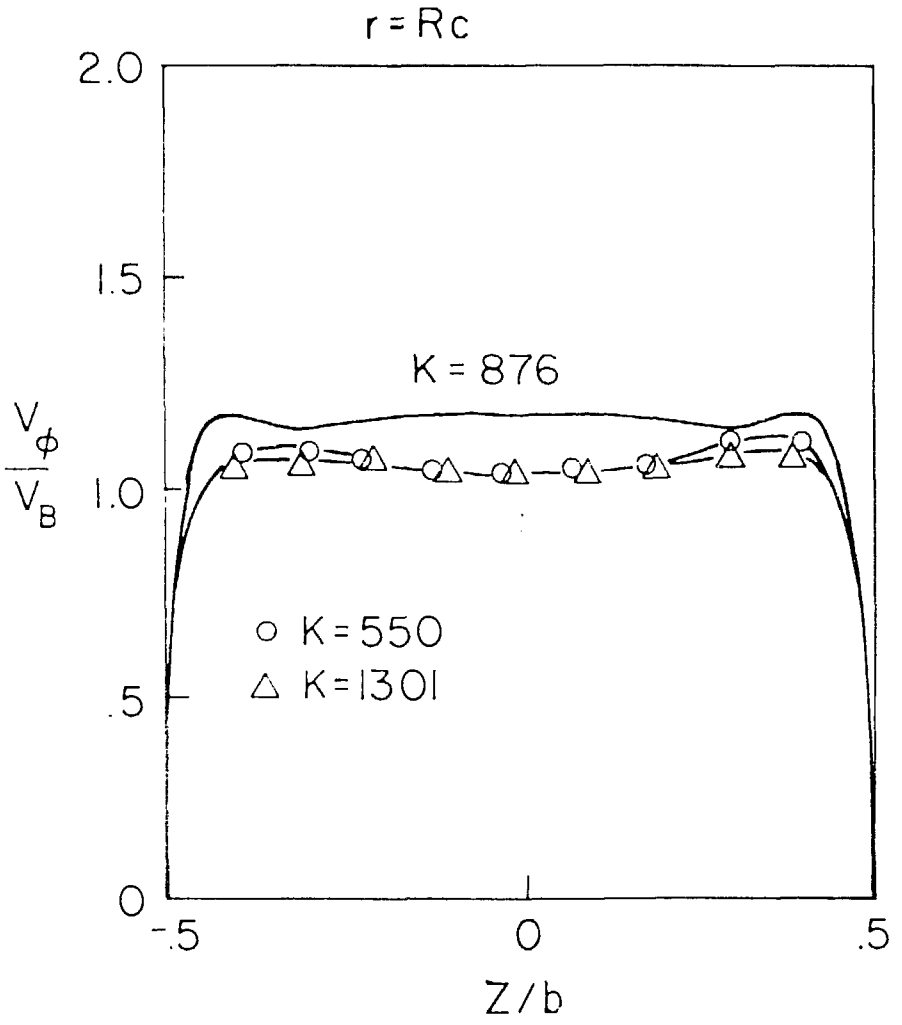

FIGURE 3-b

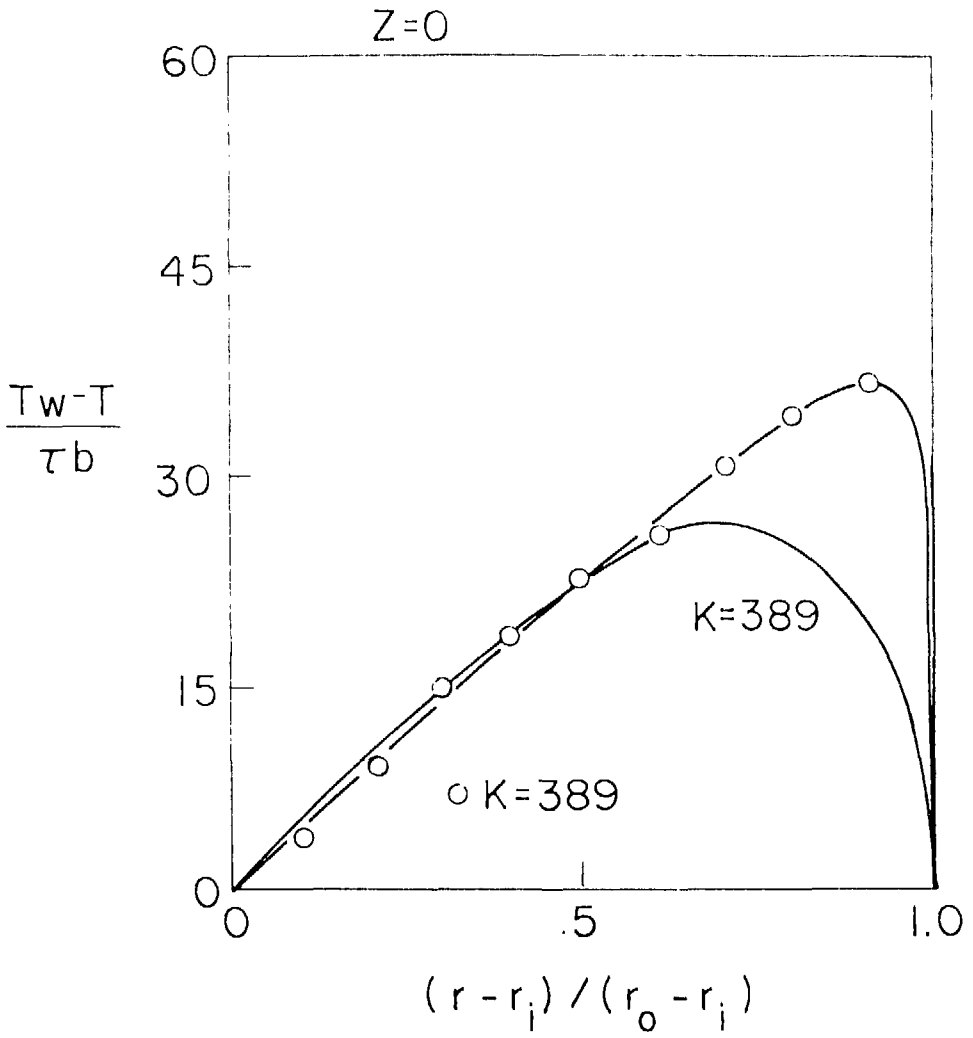

FIGURE 3-c

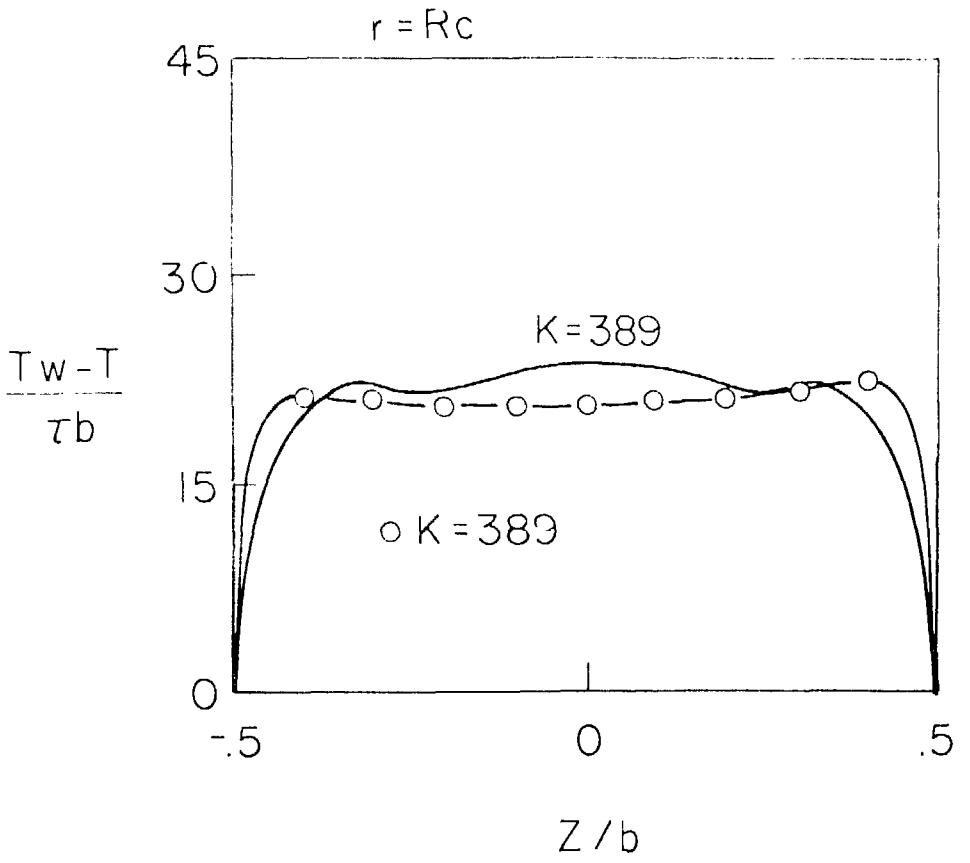

FIGURE 3-c

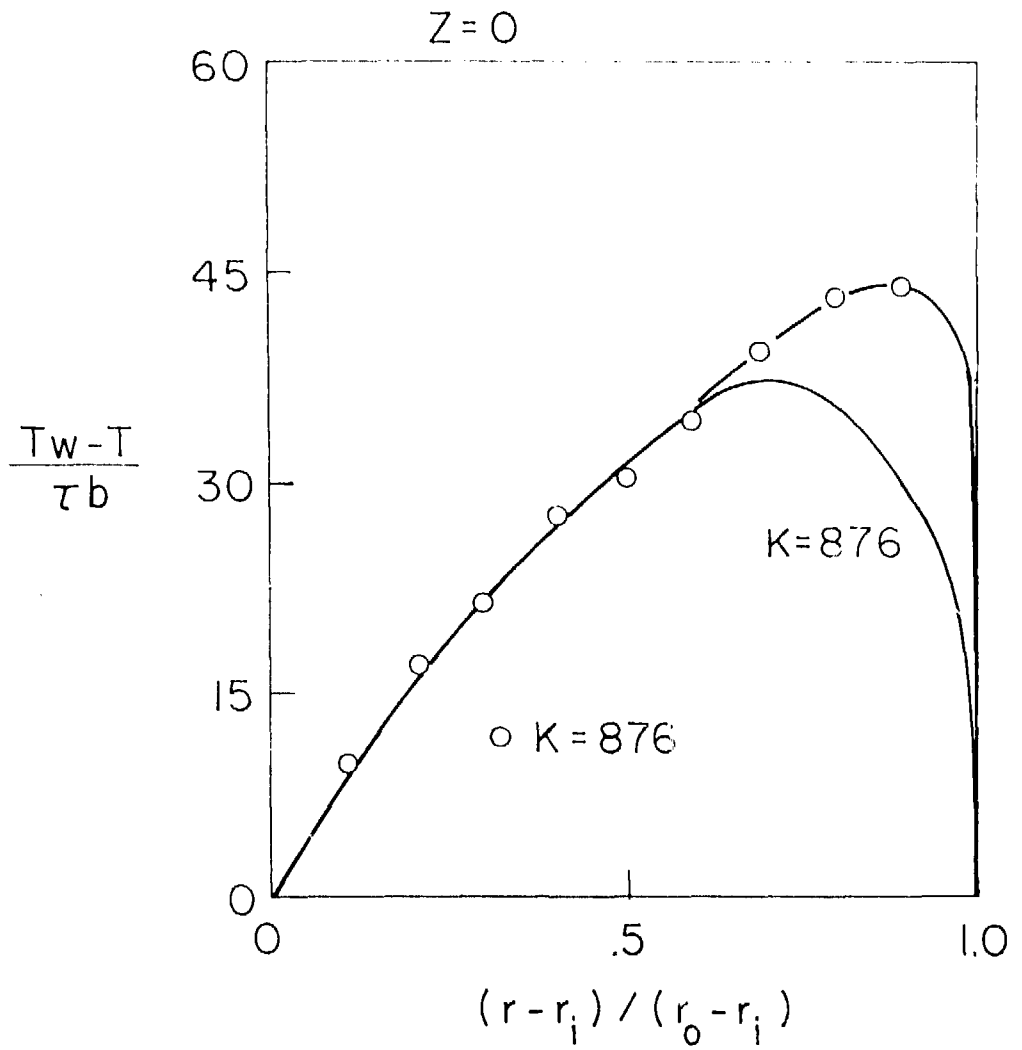

FIGURE 3-d

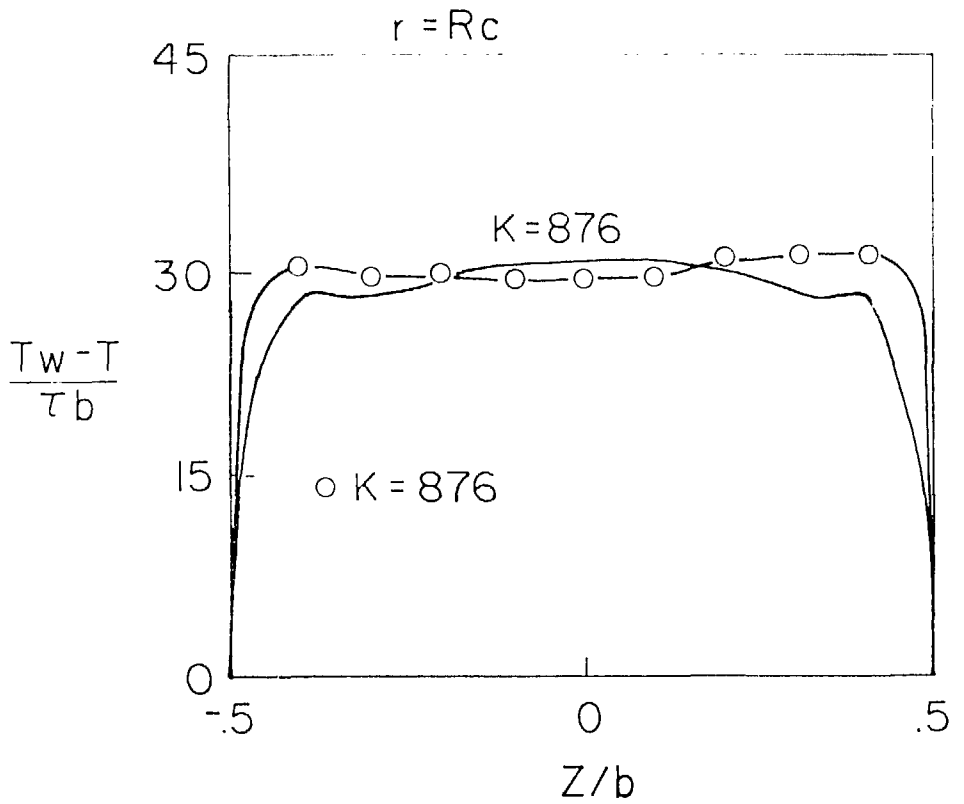

FIGURE 3-d

CONTOUR LEVELS
A 2.00E-01
B 4.00E-01
C 6.00E-01
D 8.00E-01
E 1.00E+00
F 1.20E+00
G 1.40E+00
H 1.60E+00
I 1.80E+00
J 2.00E+00
SCALE FOR VECTORS
1.40E-01
0.32+00
CONTOUR LEVELS
A 1.30E-03
B 2.00E-03
C 3.00E-03
D 4.00E-03
E 5.00E-03
F 6.00E-03
G 7.00E-03
H 8.00E-03
I 9.00E-03

FIGURE 4-a

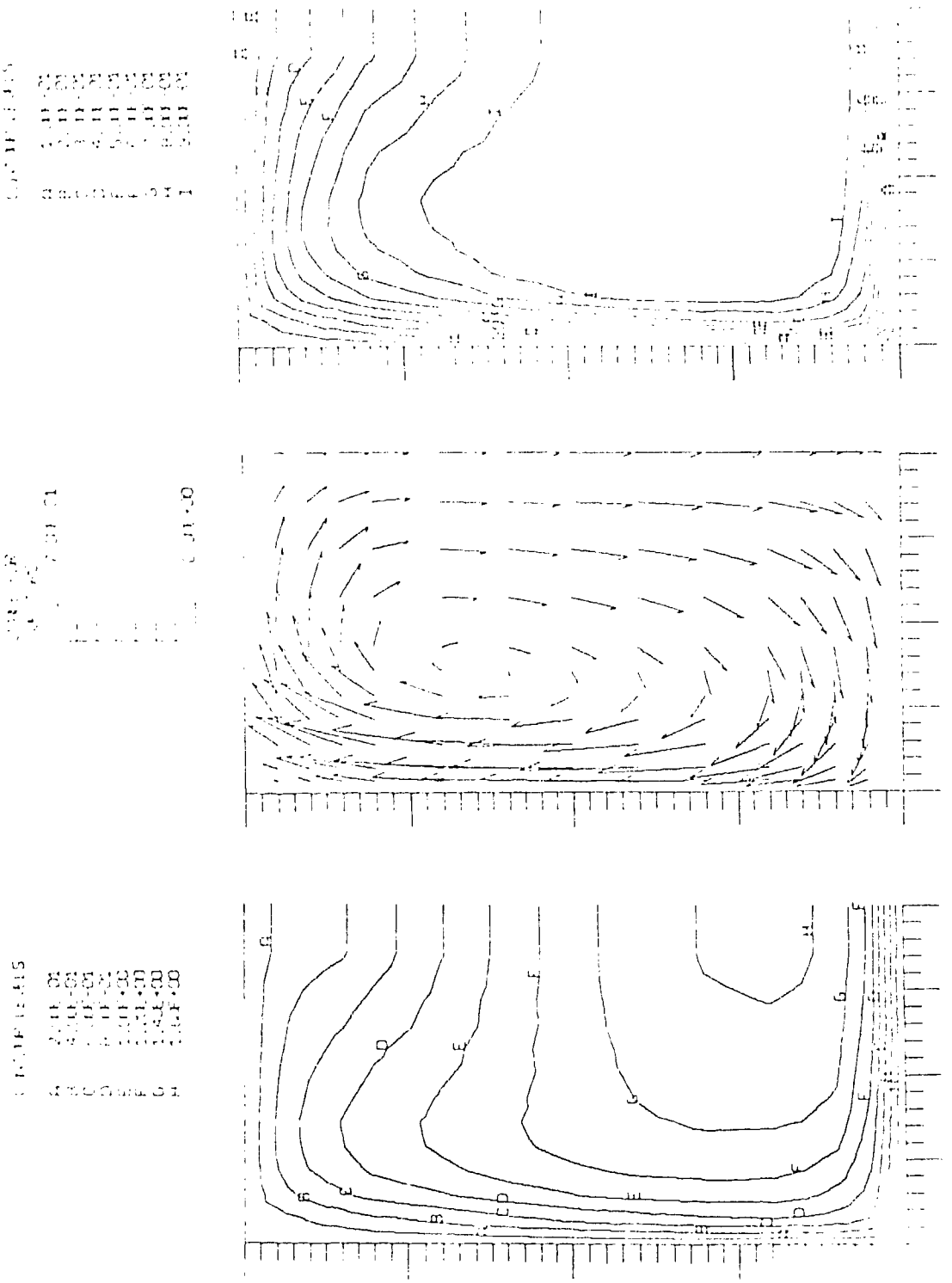

FIGURE 4-b

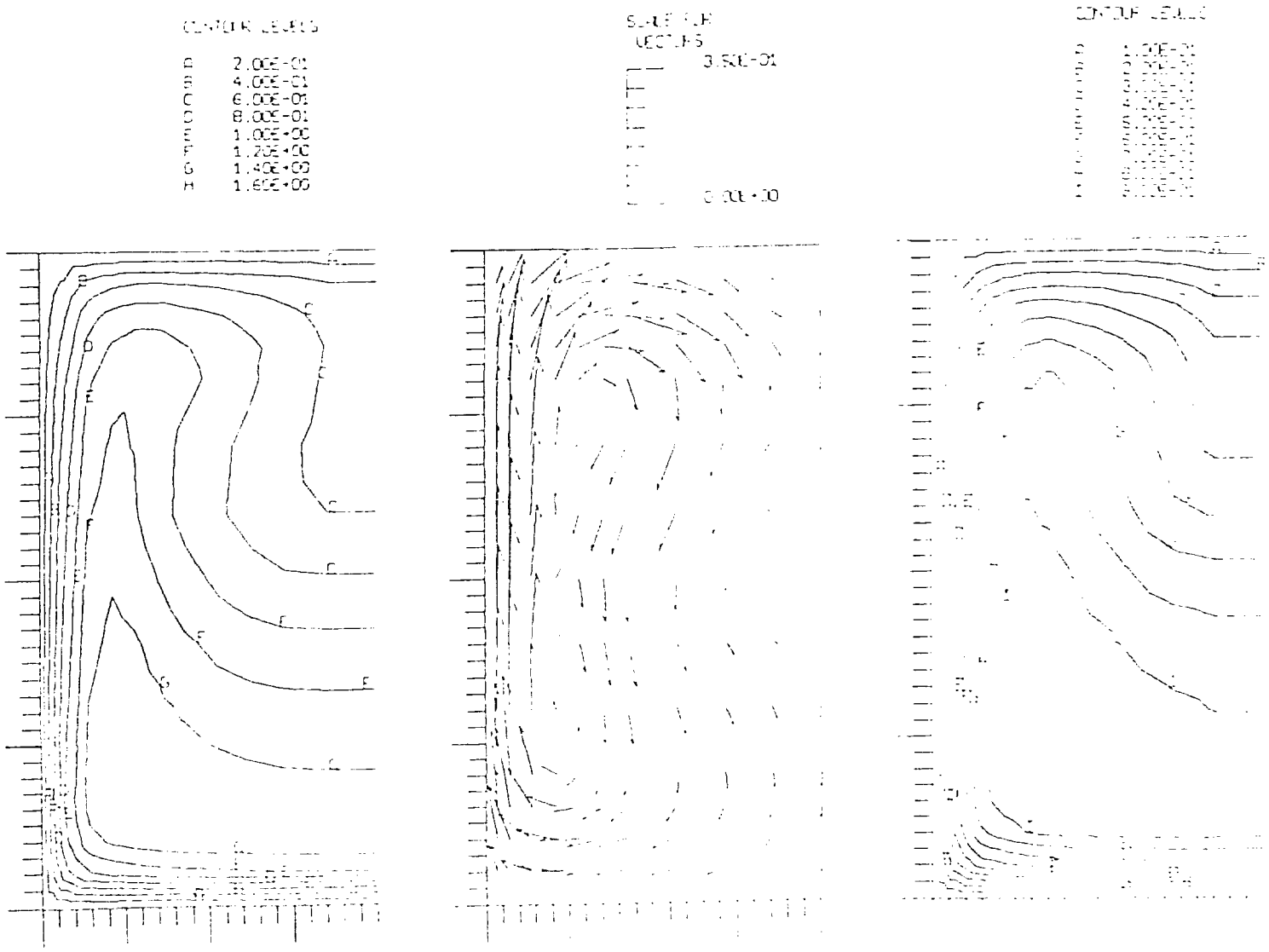
CONTOUR LEVELS
B 2.00E-01
C 4.00E-01
D 6.00E-01
E 8.00E-01
F 1.00E+00
G 1.20E+00
H 1.40E+00
I 1.60E+00
SCALE FOR
VECTORS
3.50E-01
0.00E+00
CONTOUR LEVELS

FIGURE 4-c

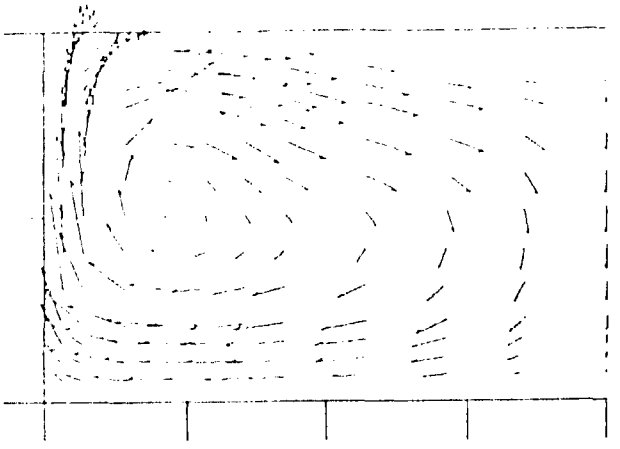

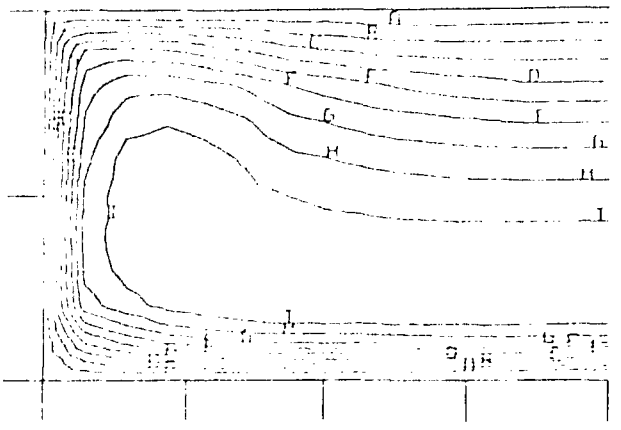

CONTOUR LEVELS

A	1.00E-01
B	2.00E-01
C	3.00E-01
D	4.00E-01
E	5.00E-01
F	6.00E-01
G	7.00E-01
H	8.00E-01
I	9.00E-01

FIGURE 4-d

FIGURE 4-e

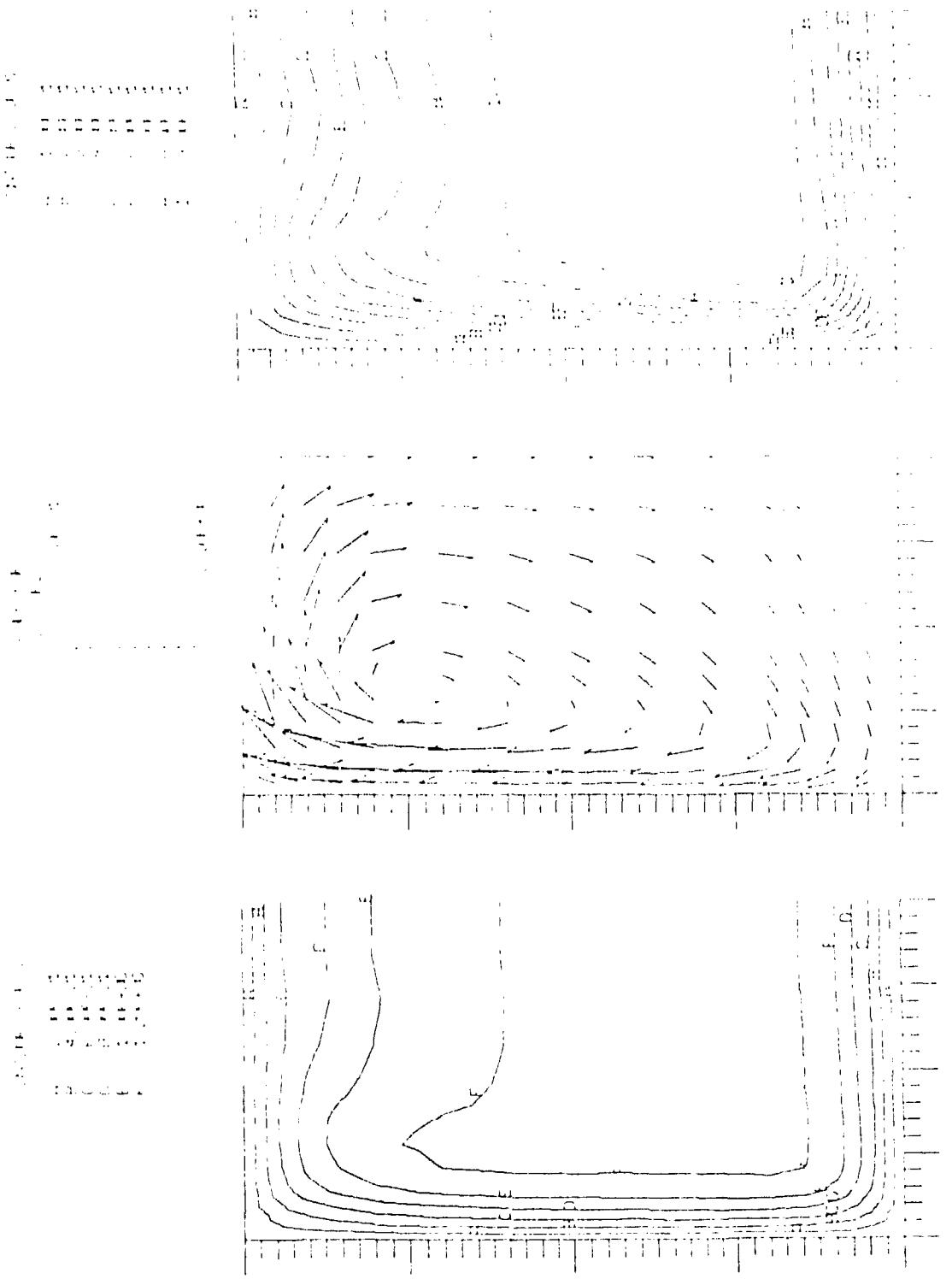

FIGURE 4-f

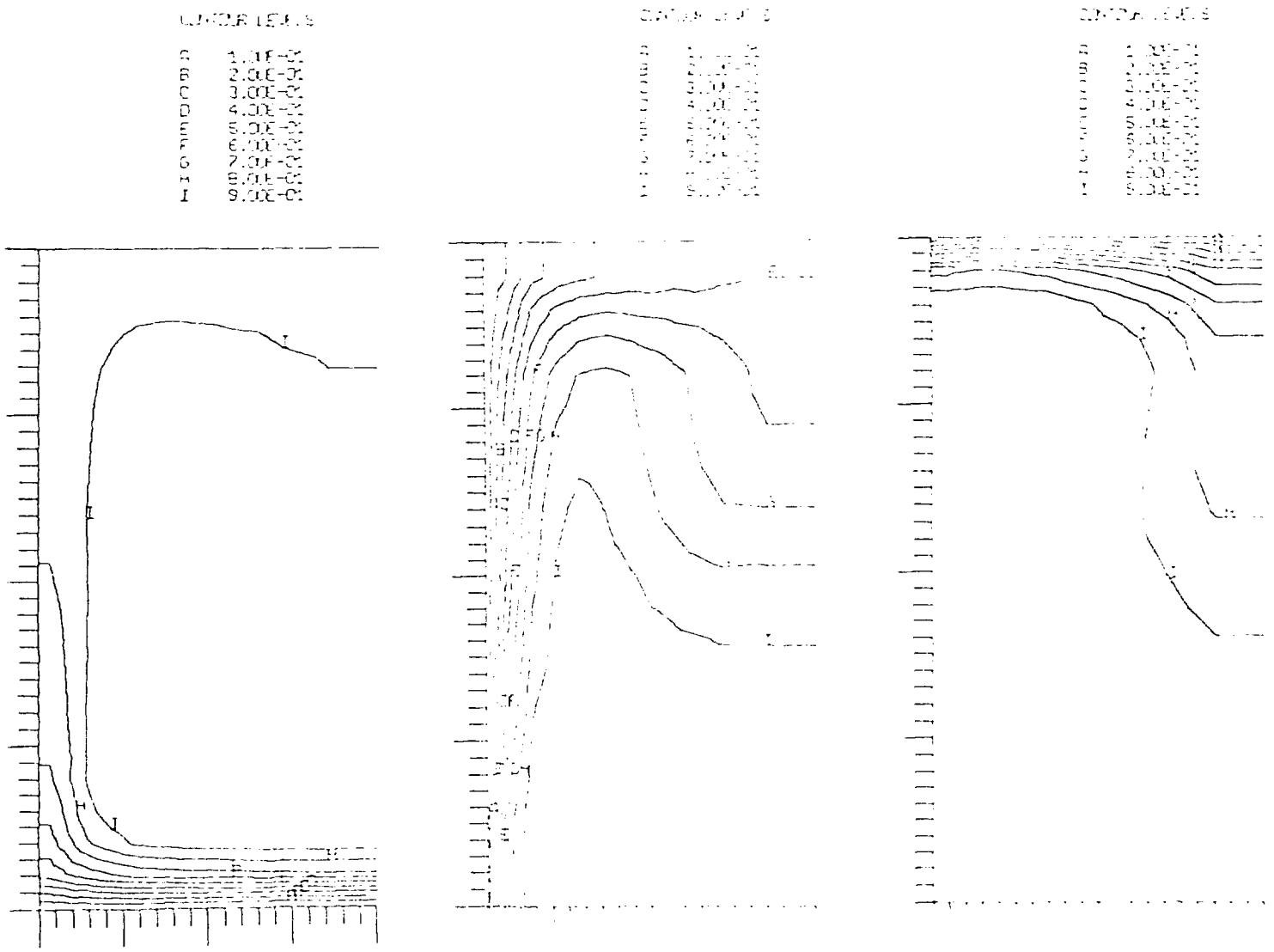

FIGURE 4-g

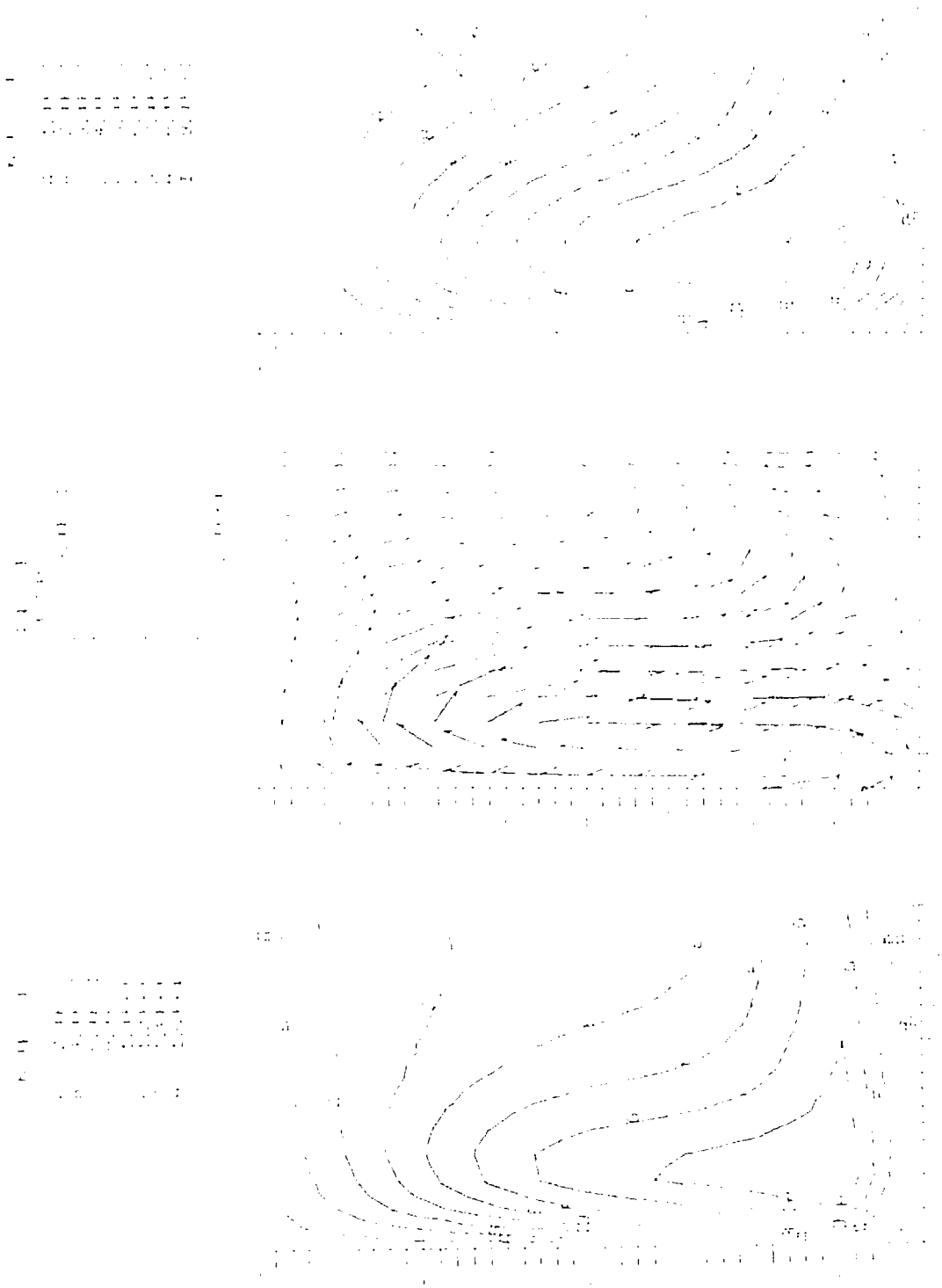

FIGURE 4-h

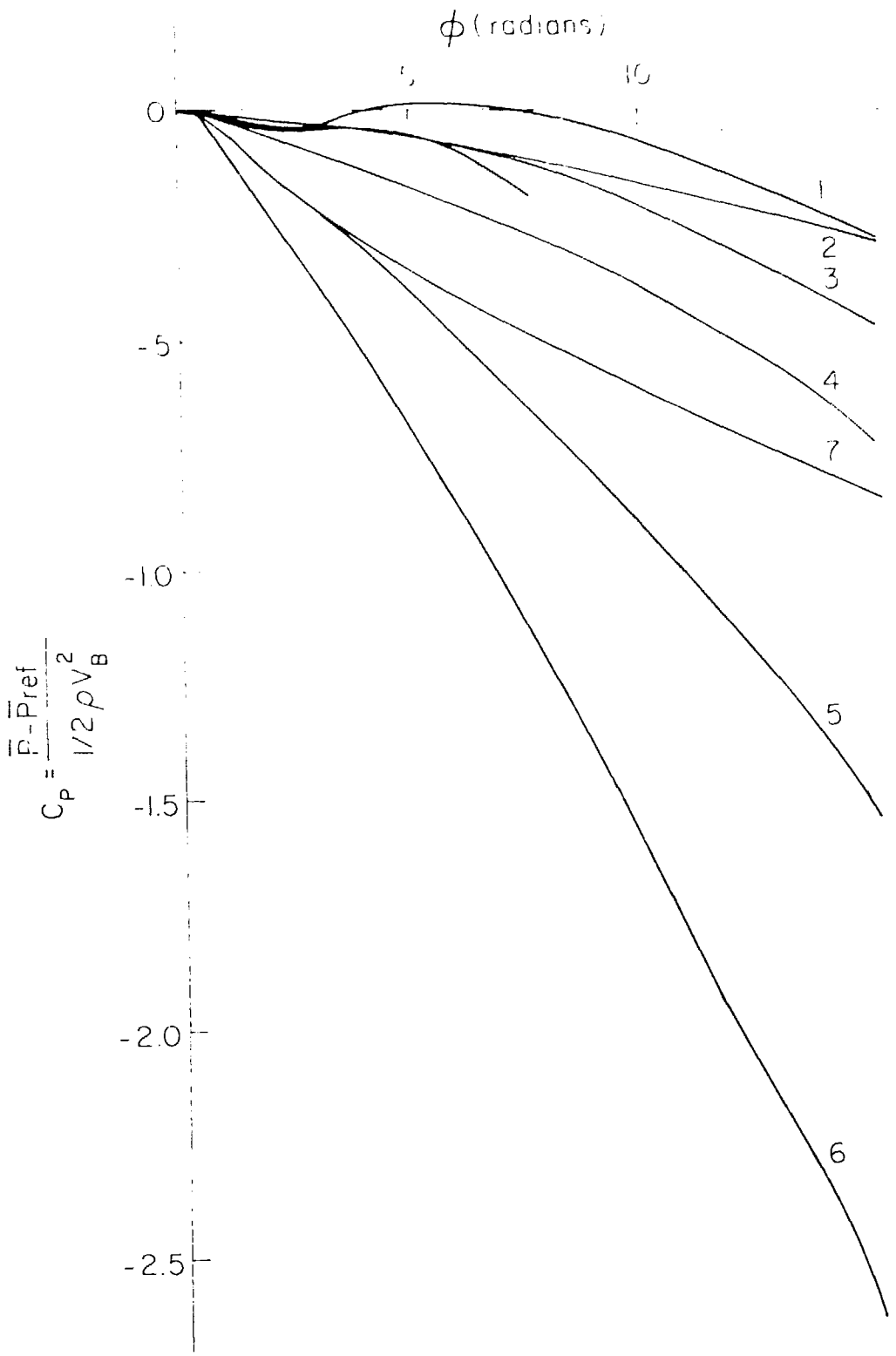
ϕ (radians)
0
-5
-10
-1.5
-2.0
-2.5
1
2
3
4
7
5
6
$C_p = \frac{\bar{P} - \bar{P}_{ref}}{1/2 \rho V_B^2}$

FIGURE 5-a

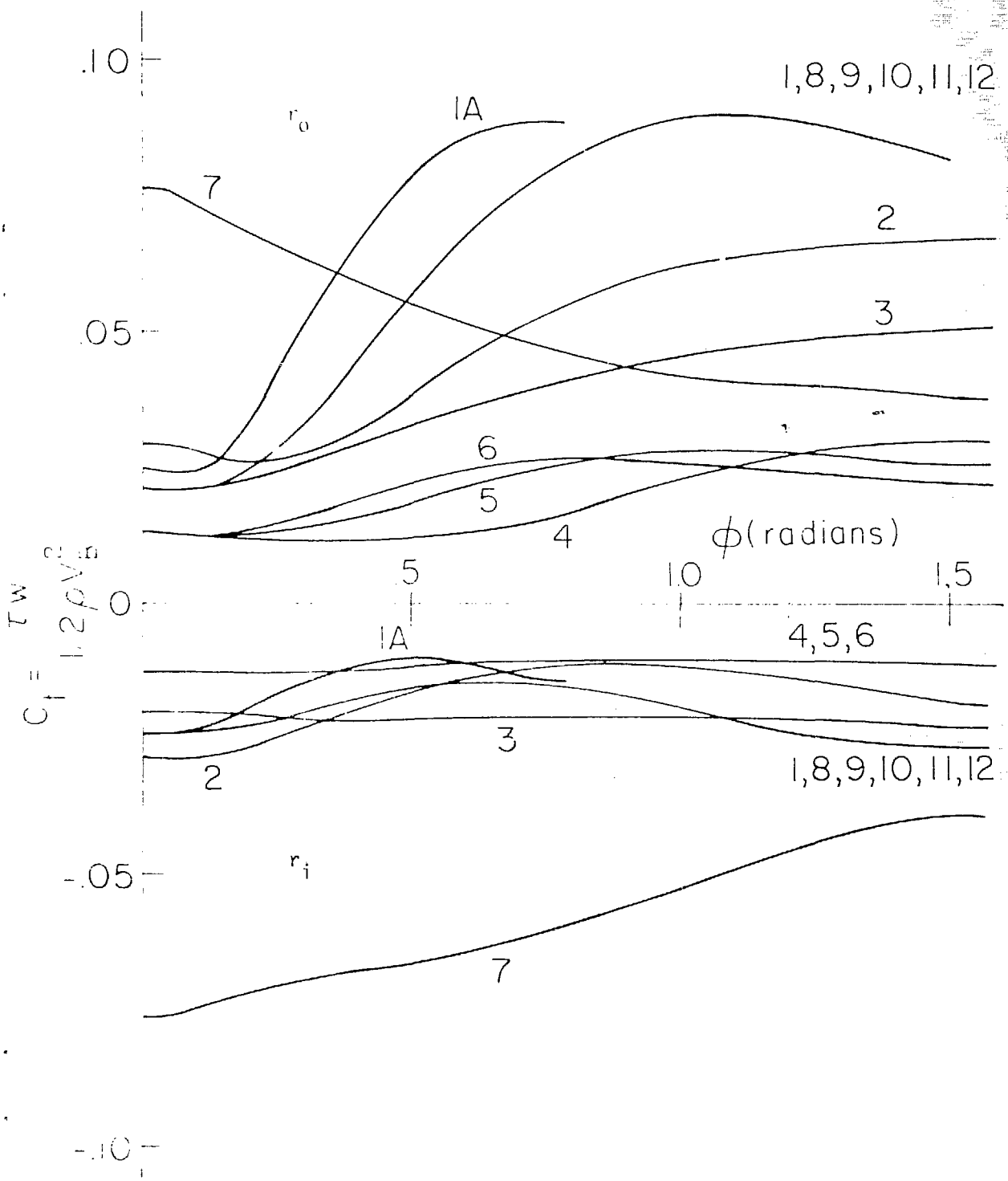
.10
.05
0
-.05
-.10
r_o
r_i
1A
7
2
3
6
5
4
1,8,9,10,11,12
ϕ(radians)
.5
1.0
1.5
4,5,6
$C_f = \frac{\tau_w}{1/2 \rho V^2}$

FIGURE 5-b

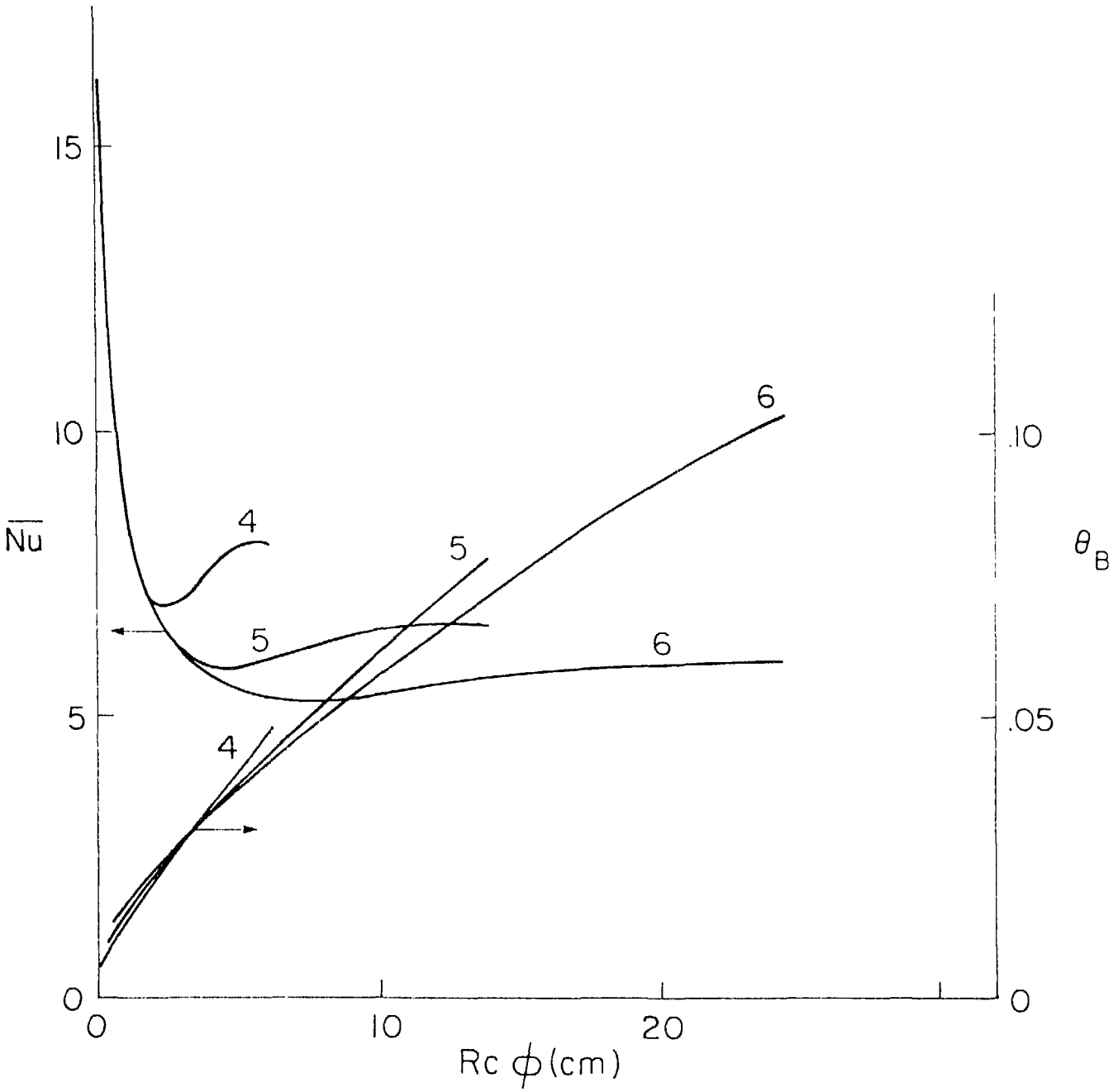

FIGURE 6-a

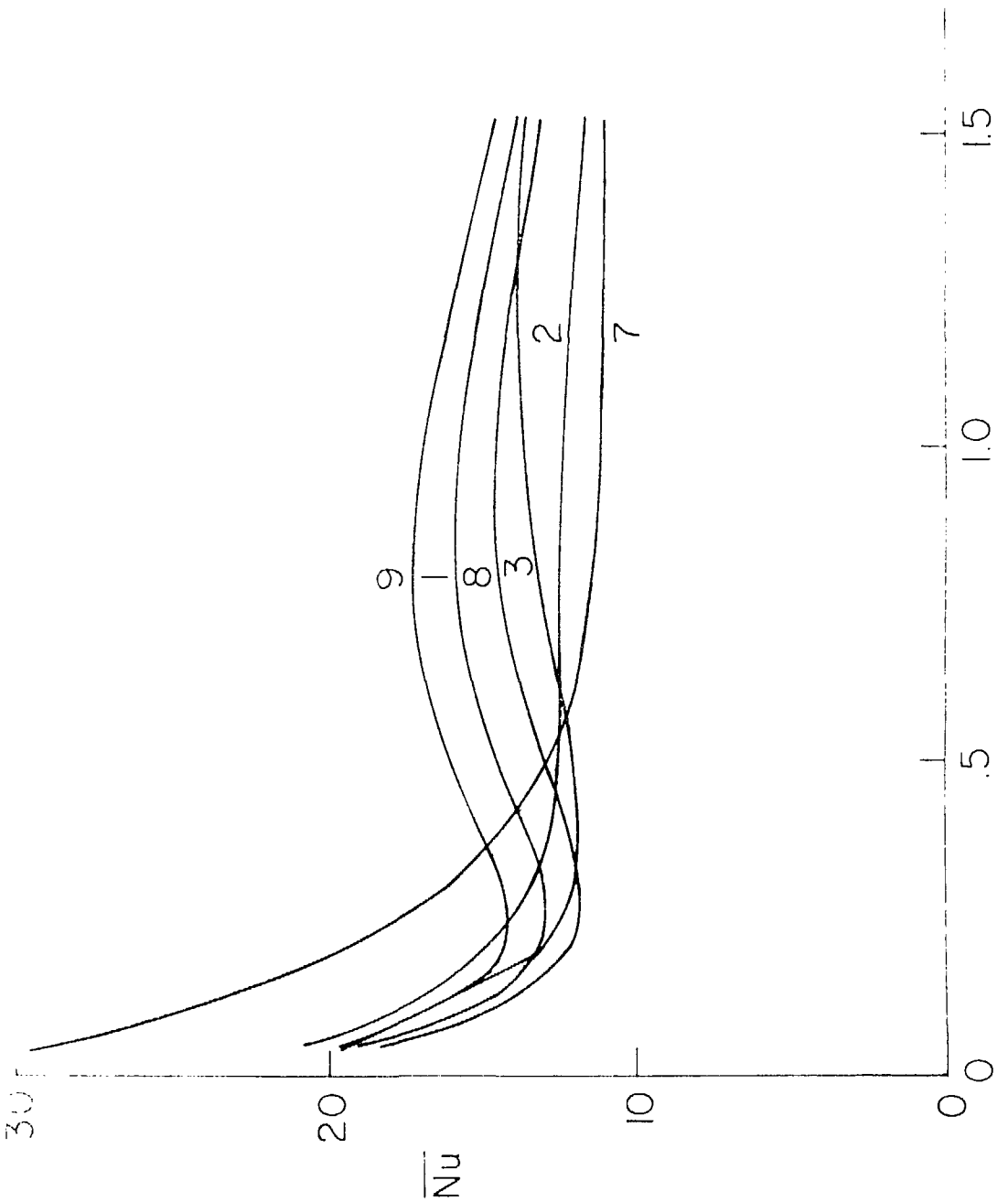

FIGURE 6-b

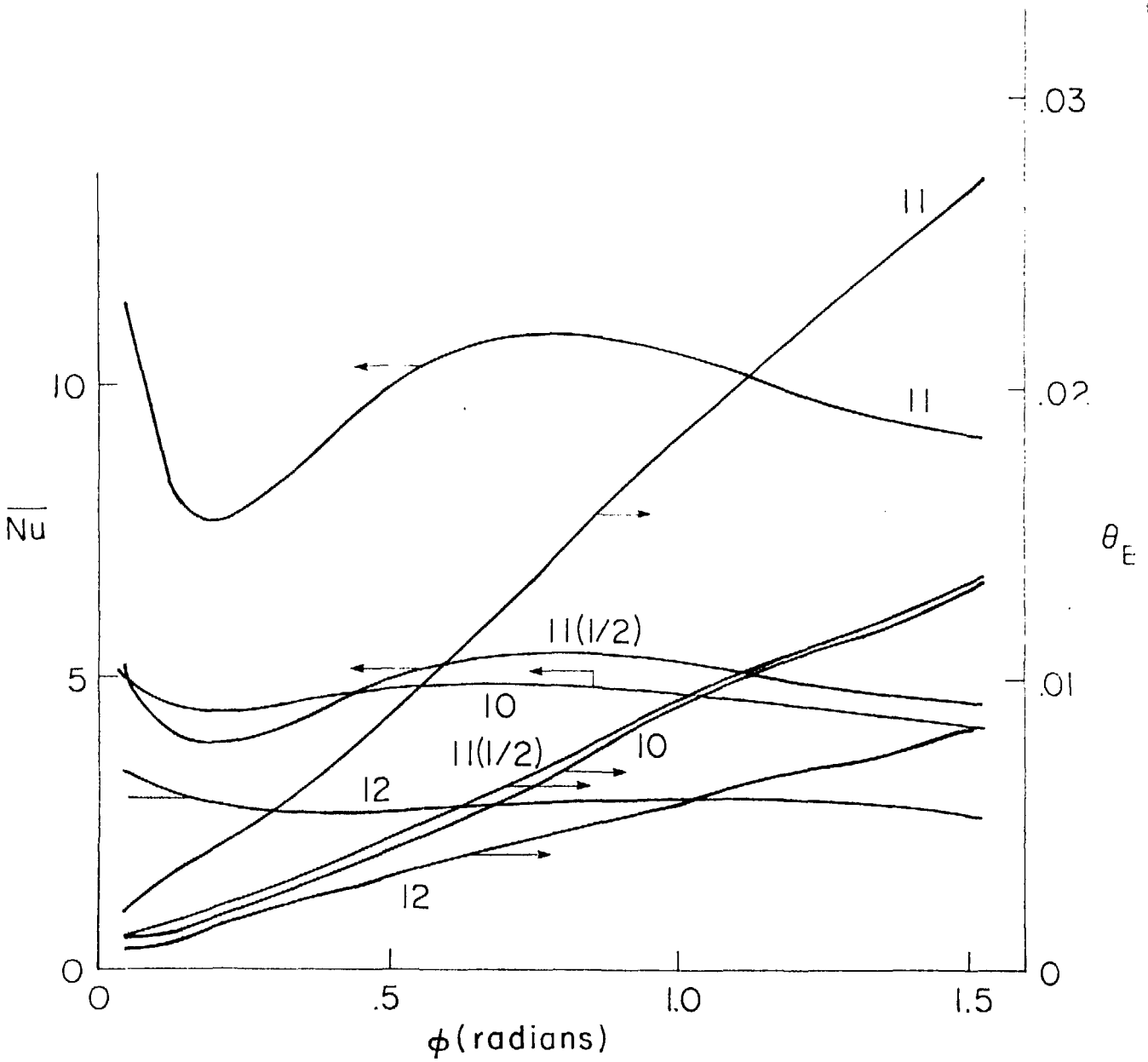
.03
.02
.01
0
10
5
0
$\overline{Nu}$
θ_E
11
11
11(1/2)
10
11(1/2)
10
12
12
0
.5
1.0
1.5
ϕ (radians)

FIGURE 6-c